AEROTHERM CORPORATION

RESEARCH & DEVELOPMENT IN AEROTHERMOCHEMISTRY

FINAL REPORT NO. 68-38, PART III

A NONGREY RADIATION TRANSPORT MODEL SUITABLE FOR USE IN ABLATION-PRODUCT CONTAMINATED BOUNDARY LAYERS

by

William E. Nicolet

N69-17791
(ACCESSION NUMBER)
63
(PAGES)
NASA CR-92473
(NASA CR OR TMX OR AD NUMBER)
(THRU)
1
(CODE)
33
(CATEGORY)
FACILITY FORM 602

©1966 AEROTHERM CORPORATION

NASA CR 92473

Aerotherm Report No. 68-38, Part III
Copy No. ___

FINAL REPORT

FURTHER STUDIES OF THE COUPLED CHEMICALLY REACTING BOUNDARY LAYER AND CHARRING ABLATOR

PART III

A NONGREY RADIATION TRANSPORT MODEL SUITABLE FOR USE IN ABLATION-PRODUCT CONTAMINATED BOUNDARY LAYERS

by
William E. Nicolet

Prepared for

NATIONAL AERONAUTICS AND SPACE ADMINISTRATION

October 15, 1968

CONTRACT NAS9-6719

Technical Management
NASA Manned Spacecraft Center
Houston, Texas
Structures and Mechanics Division
D.M. Curry
G. Strouhal

ABSTRACT

This report describes a prediction method which can be used to obtain nongrey radiative fluxes or intensities at any point within a plane-parallel slab (for the flux calculation) or at any point on a ray (for the intensity calculation). The method was developed for the study of radiation heating phenomena in the mass injected, hypersonic boundary layer environment; however, it is not limited to such studies. The radiative properties model assumes local thermodynamic equilibrium and considers the continuum transitions, molecular bands and atomic lines of the species of the C-H-O-N elemental system. The smeared line model for the molecular bands is the only approximation which is an integral part of the method. Any of the other aspects of the properties model can be made to include as much (or little) detail as desired, allowing trade-offs to be made between accuracy and computational effort.

FOREWORD

The present report is one of a series of four reports, published simultaneously, which describe extension and application of analyses and computational procedures for predicting the in-depth response of charring ablation materials and nonsimilar chemically reacting boundary layers which were generated under a previous contract (NAS9-4599). In particular, the present reports describe the extension of a laminar multicomponent chemically-reacting (equilibrium) boundary-layer program to include nongrey radiation coupling, the extension of this computational procedure to turbulent flow (at this point for incompressible flows only), the further checkout of a code which couples the laminar boundary layer procedure to a transient charring ablation code, and the application of these and other computational procedures to the Apollo heat shield material and typical Apollo missions. Part I serves as a summary report and describes the present status of and solutions obtained with the various computational procedures. In Part II a thermochemical ablation program based on a transfer-coefficient approach is utilized to investigate ablation mechanisms for the Apollo heat shield material. The radiation transport model which is utilized is described in Part III, whereas the turbulent boundary layer code is discussed in Part IV.

The titles in the series are:

Part I: Summary Report: Further Studies of the Coupled Chemically Reacting Boundary Layer and Charring Ablator, by E.P. Bartlett, W.E. Nicolet, L.W. Anderson, and R.M. Kendall.

Part II: An Evaluation of Surface Recession Models for the Apollo Heat Shield Material, by E.P. Bartlett, and L. W. Anderson.

Part III: A Nongrey Radiation Transport Model Suitable for Use in Ablation-Product Contaminated Boundary Layers, by W. E. Nicolet

Part IV: Nonsimilar Solution of an Incompressible Turbulent Boundary Layer by an Integral Matrix Method, by L. W. Anderson and R. M. Kendall.

This effort was conducted for the Structures and Mechanics Division of the Manned Spacecraft Center, National Aeronautics and Space Administration under Contract NAS9-6719 with Mr. Donald M. Curry as the NASA Technical Monitor. Development of the turbulent boundary layer code was sponsored jointly by NASA/MSC and by the Air Force Weapons Laboratory, Kirtland Air Force Base, with Lt. Ronald H. Aungier as Project Engineer. Extension of the turbulent boundary layer analysis to compressible flows is continuing under AFWL sponsorship. Mr. Eugene P. Bartlett of Aerotherm Corporation was Program Manager and Principal Investigator for the efforts reported here.

TABLE OF CONTENTS

Section	Title	Page
	ABSTRACT	ii
	FOREWORD	iii
	LIST OF TABLES	v
	LIST OF FIGURES	v
	LIST OF SYMBOLS	vii
1	INTRODUCTION	1
2	ABSORPTION COEFFICIENTS OF THE BOUNDARY LAYER SPECIES	2
	2.1 Important Absorption Mechanisms	2
	2.1.1 Atomic Continuum Transitions	2
	2.1.2 Atomic Line Transitions	4
	2.1.3 Molecular Band Transitions	9
	2.1.4 Other Transitions	12
	2.2 The Radiation Properties Model	14
	2.2.1 Molecular Band Model	14
	2.2.2 Atomic and Ionic Line Model	14
	2.2.3 Sources of Data	15
3	TRANSPORT MODEL	18
	3.1 Formulation	18
	3.2 Evaluation of Flux Integrals	21
	3.2.1 Nodal Points in Frequency	22
	3.2.2 Nodal Points in Space	24
	3.2.3 Integration Scheme	25
	3.3 The Radiation Transport Program (RAD)	25
4	APPLICATION OF THE METHOD	26
	4.1 Comparison with Other Predictions	26
	4.2 Comparisons with Measured Data	32
	4.3 Application to Uniform Slabs	38
	4.4 Application of Nonuniform Slabs	38
5	CONCLUDING REMARKS	51
6	REFERENCES	52

LIST OF TABLES

Number	Title	Page
I	Atomic and Ionic Continuum	15
II	Atomic and Ionic Lines	16
III	Molecular Band Systems	17
IV	Other Contributors	17

LIST OF FIGURES

Number	Title	Page
1	Continuum Cross Sections of Nitrogen	5
2	Typical Absorption Coefficient Predictions Including Important Molecular Contributions	11
3	Coordinate System	19
4	Spatial Grid Transformations	24
5	Comparison with the Predictions of Morris et.al. (Ref. 39)	27
6	Effect of N^- on the Spectral Distribution of the Intensity of Nitrogen, δ = 1 cm	28
7	Flux Emitted from a Uniform Air Slab, P = 1 atm	30
8	Flux Emitted from a Uniform Air Slab, P = 1 atm	31
9	Intensity Emitted from a Uniform Nitrogen Slab, δ = 1 cm	33
10	Intensity Emitted from a Uniform Hydrogen Slab, T = 10,000°K	34
11	Comparison with the Shock Tube Data of Nerem (Ref. 50), P_1 = 1 mm Hg	35
12	Comparison with the Shock Tube Data of Nerem (Ref. 50), P_1 = 2 mm Hg	36
13	Comparison with Shock Tube Data of Gruszynski and Warren (Ref. 51)	37
14	Comparison with Shock Tube Data of Wood (Ref. 53) and Wood et.al. (Ref. 52)	39
15	Comparison with Total Intensity Measurements of Wood (Ref. 53) and Wood et.al. (Ref. 52)	40
16	Variation of Flux from a Uniform Air Slab, δ = 1 cm	41

LIST OF FIGURES (concluded)

Number	Title	Page
17	Variation of Flux from a Uniform Air Slab, δ = 10 cm	42
18	Thermodynamic State Variation	43
19	Spatial Distribution of Radiating Species	45
20	Spectral Distribution of Continuum Fluxes	46
21	Spectral Variation of Positive Flux at Wall	47
22	Positive Flux Variation	49
23	Net Flux (Positive When Directed Toward the Wall)	50

LIST OF SYMBOLS

B	Planck function
b	line shape function
C	constant
c	speed of light
E	black body emissive power
e	charge on an electron
$\mathcal{E}_n$	exponential integral of order n
$F^{\pm}$	one sided radiative flux
f	oscillator strength of a line (f-number)
f	growth parameter (Eqs. (35) and (37))
f_1, f_2	arbitrary constants (Eqs. (34) and (35))
g	Gaunt factor
h	Planck's constant
j	emission per unit volume
k	Boltzmann's constant
m	mass of an electron
N_1, N_L	number of quantities, Eq. (1)
N	number density
n	principal quantum number
Q	partition function
q	net flux
Ry	Rydberg constant
S	line strength
X	ionization potential
y	spatial coordinate
$\bar{y}$	a particular spatial point

GREEK SYMBOLS

β	defined as hRy/kT
Γ	partition function ratio

LIST OF SYMBOLS (concluded)

γ	line half width
δ	path length
ϵ	emissivity
μ	absorption coefficient
μ'	absorption coefficient corrected for induced emission
ν	photon frequency
ξ	Gaunt-like correction factor for non-hydrogenic atoms
τ	optical depth
φ	stretching parameter (Eq. (38))

SUBSCRIPTS

bf	bound free transition
c	quantity evaluated at the center of a line
ff	free free transition
i	species i
j	abosrbing level j
k	line k
δ	quantity evaluated at the outer edge of the layer
ν	spectral quantity

SUPERSCRIPTS

C	continuum quantity
D	quantity due to the Doppler effect
FF	free free transition
L	line property
PD	photodetachment transition
R	quantity due to the resonance effect
S	quantity due to the Stark effect
^	lowest level to be included in integral formulation
~	highest level allowed under given plasma condition
—	averaged quantity

A NONGREY RADIATION TRANSPORT MODEL SUITABLE FOR USE IN ABLATION-PRODUCT CONTAMINATED BOUNDARY LAYERS

SECTION 1

INTRODUCTION

The ability to predict radiant energy transfer is required in order to understand the heating phenomena associated with bodies entering planetary atmospheres at high velocities. The radiation transport is important both as an energy source in direct thermal contact with the body and indirectly through the coupling between it and the thermal boundary layer. Quantitative predictions of radiative transport under these conditions require frequency dependent properties of the radiating species and a frequency dependent transport model. In this study attention is directed toward a transport model which is simple enough to be used as part of a coupled flow field calculation, yet is sufficiently detailed to be able to predict the more significant features of measured spectral data.

Transport within the C-H-O-N elemental system is considered. This sytem is representative of boundary layers adjacent to most ablating bodies. Local thermodynamic equilibrium is assumed to exist at all times. Molecular, atomic and ionic species are all considered with those which appear in the 3,000°K to 15,000°K temperature range (0.1 to 10 atmospheres pressure range) being given primary consideration.

The properties utilized and the transport model are presented in Section 2 and 3, respectively. The contributions from atomic lines are particularly emphasized. Predictions of radiative heating are given in Section 4 for isothermal and nonisothermal slabs. These serve to illustrate applications of the method and, in some cases, allow for comparisons with the predictions of other investigators.

SECTION 2

ABSORPTION COEFFICIENTS OF THE BOUNDARY LAYER SPECIES

2.1 IMPORTANT ABSORPTION MECHANISMS

The spectral absorption coefficient for a plasma consisting of a mixture of elements is in general

$$\mu\nu = \sum_{i=1}^{N_1} \mu_i^C(\nu) + \sum_{k=1}^{N_L} \mu_k^L(\nu) \qquad (1)$$

where the first term represents the continuum contribution with its summation taken over all continuum transitions (N_1), and the second term represents line contributions with the summation taken over all the lines (N_L). For the plasma conditions of interest, the important continuum transitions include atomic photoionization, photodetachment, free-free transitions, photodissociation and molecular photoionization in approximately a decreasing order of importance. The atomic line transitions are very important. The molecular band systems can be important for some conditions.

2.1.1 Atomic Continuum Transitions

In general, continuum contributions depend on the plasma state (to a satisfactory approximation) only through the populations of the absorbing levels, viz.

$$\mu_i^C(\nu) = \sum_j N_{ij}\sigma_{ij}^C(\nu) \qquad (2)$$

where N_{ij} is the number density of the absorbing level and $\sigma_{ij}^C(\nu)$ is its cross-section. The number densities must be obtained from thermodynamic state calculations and the cross sections either from quantum mechanical calculation or experiment.

Hydrogen cross sections are well understood, exact values being available (Ref. 1)

$$\sigma_{\ldots} = \frac{2^6\pi^4}{3\sqrt{3}} \frac{me^{10}}{ch^6 n_a^5 \nu^3} g_{bf} \qquad (3)$$

$$\sigma_{ff} = \frac{2^4 \pi^2 e^6}{3\sqrt{3}\, hc(2\pi m)^{3/2}} \frac{N_e}{(kT)^{1/2}\nu^3} g_{ff} \qquad (4)$$

where the subscripts bf and ff refer to bound-free (photoionization) and free-free transition, respectively. The quantity n_a is the principal quantum number of the absorbing level; N_e is the number density of free electrons; g_{bf} and g_{ff} are Gaunt factors which are available in tabular form (Ref. 1), and the other symbols have their usual meanings. The Gaunt factors are often taken to be unity (a good approximation) or expressed in terms of shell averages ($\bar{g}_{ff}$). This allows a closed form expression to be obtained for the free-free contribution for the z,z+1 stage of ionization (Ref. 2), viz.

$$\mu_i^{FF}(\nu) = \frac{32}{3\sqrt{3}} \left(\frac{\pi^2 e^6}{2hc}\right) \frac{kT(z+1)^2}{(h\nu)^3} \frac{Q^{z+1}}{Q^z} \exp\left(-\frac{x^z}{kT}\right) \bar{g}_{ff} \qquad (5)$$

where Q^z and Q^{z+1} are the electronic partition functions of the atom and its ion, respectively, were x^z is the ionization energy of the atom, where z+1 is the charge on the residual ion. The photoionization contribution is also simplified, viz.

$$\mu_i^{PI}(\nu) = \mu_i^{FF}(\nu) \sum_{\nu_{n_a} < \nu} \frac{1}{n_a^3} \exp\left(\frac{h\nu_{n_a}}{kT}\right) \qquad (6)$$

where ν_{n_a} is the threshold frequency of the level n_a. At sufficiently high values of n_a, the levels are so closely spaces that the summation can be approximated by an integration (see Ref. 3, for example)

$$\mu_i^{PI}(\nu) \approx \mu_i^{FF} \left\{ \exp(hRy/n^2 kT) - \exp(hRy/\tilde{n}^2 kT) \right\} \qquad (7)$$

where n is the lowest level to be included in the integral formulation and $\tilde{n}$ is the highest level allowed at the given plasma condition.

In the case of the heavy atoms, no exact cross sections are available. The most widely accepted method of calculating them is the "quantum defect" approximation as put forth by Burgess and Seaton (Ref. 4). This method has been used by Armstrong, Johnston and Kelly (Ref. 5, see also Refs. 6, 7, and 8) to obtain the level cross sections for the levels of N and O. A compilation

of this work is available (Ref. 2) in which "effective cross sections" ($\equiv \mu_i(\nu)/N_i$) are tabulated.

A useful approximation for the heavy atom contributions at low frequencies has been proposed by Biberman and Norman (Ref. 6). They also use the quantum defect method but have obtained an approximate, closed form solution for the total contribution. Their results are presented in terms of two correction factors to be applied to the hydrogenic formula, viz.

$$\mu_i^{PI,FF}(\nu) = \Gamma\xi(h\nu,T)\left[\mu_i^{PI,FF}(\nu)\right]_{\text{hydrogenic}} \tag{8}$$

where $\Gamma = 2Q^{z+1}/Q^z$. Tabulated values of $\xi(h\nu,T)$ are available (Ref. 6) for many different atoms. The absorption coefficients calculated from Equation (8) show surprisingly good agreement with the fully detailed ones of Armstrong et.al.(Ref. 5). Tabulated values of the effective cross sections of C and C+ as obtained from Equation (8) are available (Ref. 2).

Figure 1 shows nitrogen continuum cross sections taken from References 5 and 6 and illustrates the dominant importance of the photoionization edges.

2.1.2 Atomic Line Transitions

The absorption coefficients of the atomic line transitions depend on the plasma condition both through the population of the absorbing level and also through the shapes of the lines. Thus,

$$\mu^L_{k(j)}(\nu) = \frac{\pi e^2}{mc} f_{k(j)} N_{ij} b_{k(j)}(\nu,T,P,x_1,x_2\ldots) \tag{9}$$

where $f_{k(j)}$ is the oscillator strength of the k^{th} line in the j^{th} series of lines and $b_{k(j)}(\nu,T,P,x_1,x_2,\ldots)$ is the line shape and is a function of frequency and the plasma condition. The line shape obeys the normalization condition (omitting the explicitly written functional dependence on the plasma condition for brevity)

$$\int_0^\infty b_k(\nu)\,d\nu = 1$$

but otherwise is free to take on a variety of functional forms depending upon the species involved and the broadening mechanisms (or combination of mechanisms).

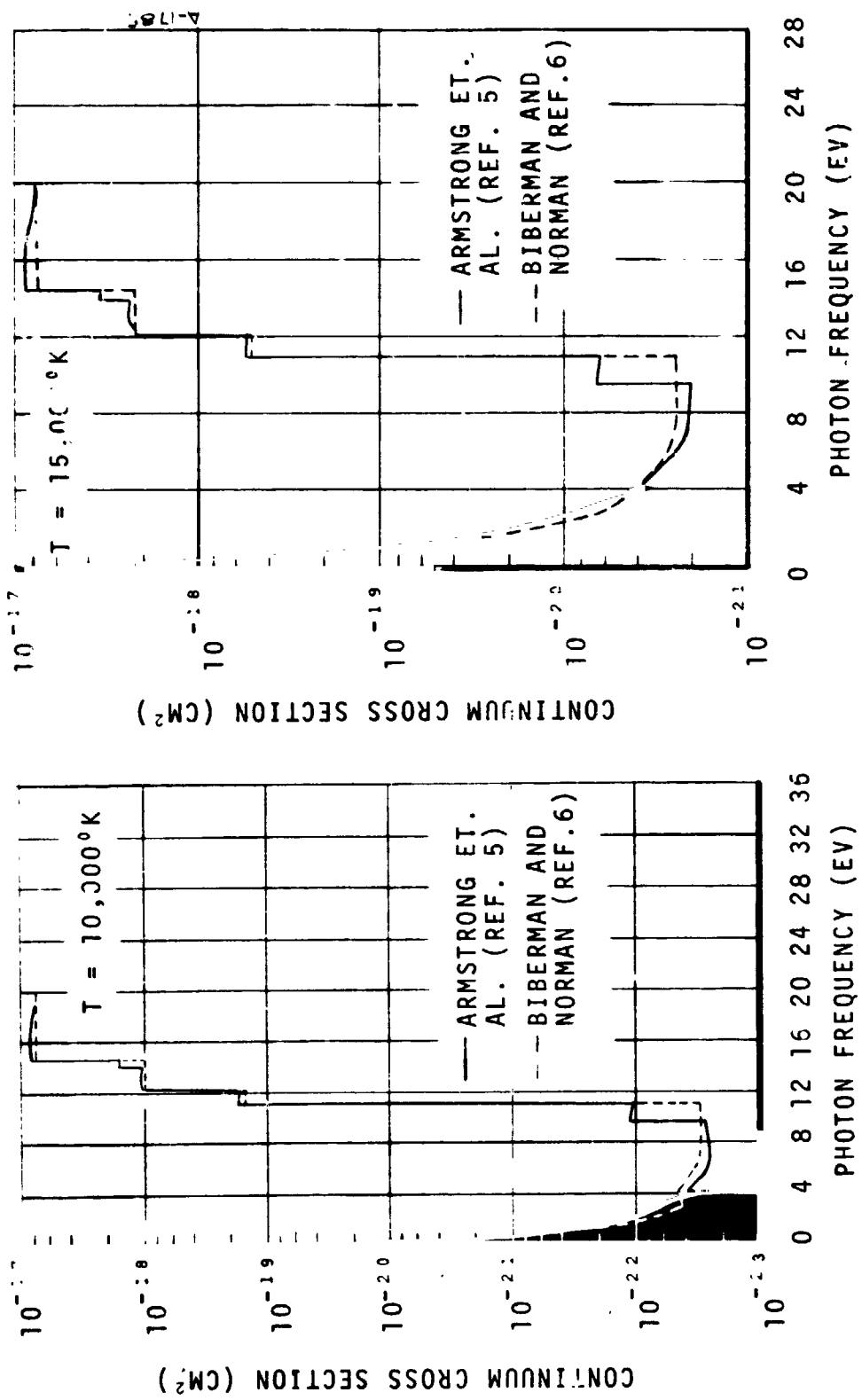

Figure 1. Continuum Cross Sections of Nitrogen

For the heavy atomic species, the dominant broadening mechanism is Stark broadening by electron impacts. Following Armstrong et.al.(Ref. 5) it is assumed that each multiplet can be treated as a line with a Lorentz shape, viz.

$$b_k(\nu) = \frac{\gamma_k^S/\pi}{(\nu-\nu_k)^2 + (\gamma_k^S)^2} \tag{10}$$

where ν_k is the frequency of the line center and γ_k^S is the Stark (half) half-width which is a function of the plasma condition. Corrections to Equation (10) due to J-splitting and effects due to ion perturbers are often ignored.

The (half) half-widths, γ_k^S, can be calculated from the electron impact approximation. Griem (Ref. 9) has worked out the proper formulation and tabulates data for many transitions and for several elements. Wilson and Nicolet (Ref. 2) have performed the calculations* for all the important transitions in N, N+, O, O+, C and C+. A comparison given by Wilson and Greif (Ref. 10) shows that the data of Reference 2 compares favorably with that of Reference 9. Page et.al.(Ref. 11) report that the (half) half-widths from Reference 2 can be approximated as

$$\gamma_k^S \approx \gamma_k^S\left(T_o\right)\left(\frac{T}{T_o}\right)^n \tag{11}$$

where n = 0.25 and 0.46 for nitrogen and oxygen, respectively.

For many plasma conditions of present interest, the degree of ionization is very low. Under such conditions, resonance broadening can be greater than Stark broadening, yielding lines with Lorentz shapes having (half) half-widths which can be calculated in an impact approximation (Ref. 15) as

$$\gamma_k^R \cong 3\pi\left(\frac{g_\ell}{g_u}\right)\left(\frac{e^2 f_{res}}{2\pi m \nu_{res}}\right)N_a \tag{12}$$

Here f_{res}, ν_{res}, g_ℓ and g_u all belong to the resonance line and are, respectively, the absorption oscillator strength, the center frequency, the lower statistical weight and the upper state statistical weight. N_a is the number of perturbing atoms per unit volume.

*It should be noted that until recently an erronious approximation was usually made in this calculation (see Ref. 2 for a discussion of this point) which resulted in half-widths which were much too large.

The broadening mechanisms for atomic hydrogen require exceptional treatment. The Stark splitting of hydrogen lines is much greater than that of other spectra (Ref. 12). This effect is connected with the accidental degeneracy in hydrogen whereby terms of the same principal quantum number but different orbital quantum numbers have (very nearly) the same energy. Further, it is known that broadening caused by ion perturbers is not negligible compared to that caused by electron impacts (see Ref. 13). Thus, the Lorentz line shapes cannot be used. The line shape in the core region of each of the important hydrogen lines was obtained by Griem, Kolb and Shen (Ref. 13) and is available in numerical form. Asymptotic equations are given by Griem (Ref. 9) for the shape of the far wings, viz.

$$b_k(\nu) = \text{const.} \frac{S_k(\alpha(\nu))}{\nu^2 \sqrt{2.61 e N_e^{.667}}} \tag{13}$$

and

$$\lim_{\alpha \to \infty} S_k(\alpha) = \frac{C_k}{\alpha^{5/2}} \left[1 + \sqrt{2.61 e N_e^{.667}} R_k(N_e, T)\right] \tag{14}$$

The parameter $\alpha(\nu)$ is defined as

$$\alpha_\nu(\nu) = \frac{C(\nu - \nu_k)}{2.61 \times 10^{-8} \nu_k^2 e N_e^{.667}} \tag{15}$$

and values of C and R are available in Ref. 9. For transitions involving highly excited levels, Griem (Ref. 14) has shown that electron impact broadening is dominant. Thus, the Lorentz shape can be used with the (half) half-widths taken from Griem (Ref. 14), viz.

$$\gamma_k^S = \text{const.} N_e \log_{10}\left(\frac{3 \times 10^6 T}{n_u^2 N_e}\right) \frac{n_\ell^5 + n_u^5}{T^{.5}} \tag{16}$$

where n_ℓ and n_u are the principal quantum numbers of the lower and upper levels of the transition, respectively.

The lines of all the species can also be broadened by the Doppler effect. Hunt and Sibulkin (Ref. 15) have recently pointed out that it is important to include this mechanism for some plasma conditions of interest. The Doppler broadened line acquires the shape

$$b_k(\nu) = \frac{1}{\sqrt{\pi}} \frac{\sqrt{\ln 2}}{\gamma_k^D} \exp\left[- \frac{(\nu - \nu_k)^2 \ln 2}{(\gamma_k^D)^2} \right] \tag{17}$$

where γ_k^D is the Doppler (half) half-width and is given by

$$\gamma_k^D = \frac{\nu_k}{C} \sqrt{\frac{2kT}{m_i} \ln 2} \tag{18}$$

where m_i is the mass of the radiating particle. In order for this mechanism to participate in a meaningful way in transport calculations, γ_k^D must be very much larger than $\gamma_k^S + \gamma_k^R$. This effect occurs because the Doppler wings decay exponentially; whereas, the Lorentz wings decay quadratically, and most of the radiant energy is (usually) transported in the wings.

Some of the atomic lines can be treated like a continuum rather than individually. The high lines* in a given series always become overlapped as they approach their series limit. Armstrong (Ref. 16) has shown that the photoionization threshold can be shifted to lower frequencies to account for the contributions from these lines, viz.

$$\Delta h\nu \sim \left(N_e^2 / kT \right)^{1/7}$$

where $\Delta h\nu$ is the shift in terms of photon energy.

Lines belonging to high series** can also be treated as a continuum contribution. They become overlapped at low frequencies; in addition, they are usually weak. Integral formulations for the contributions of these lines have been obtained in a variety of investigations (Refs. 15 and 17, for example).

---

*The high lines in a series are associated with transitions which have upper levels with large principal quantum number.

**The high series are associated with transitions which have lower levels with large principal quantum numbers.

All approximate the line strengths by shell averaged hydrogenic values. This is consistent with the fully detailed calculations (Ref. 5). For a uniform and optically thin plasma, Vorobyov and Norman (Ref. 17) have obtained the total emission per unit volume (j) of all the transitions originating at or above the level k, viz.

$$j = \text{const.}\ \frac{1}{4\beta}\ \exp\left(-\frac{X^z}{kT}\right)\Gamma\left[\frac{1}{\beta}\left(\exp\frac{\beta}{n_a^2} - \exp\frac{\beta}{\tilde{n}^2}\right) - \left(n_a^{-2} - n^{-2}\right)\exp\frac{\beta}{\tilde{n}^2}\ N_i\right] \tag{19}$$

where $\beta = hRy/kT$, where z is the charge of the atom, X^z its ionization potential and $\tilde{n}$ the highest level allowed at the given plasma condition. Vorobyov and Norman (Ref. 17) do not discuss the spectral distribution of the intensities thus obtained; however, Hunt and Sibulkin (Ref. 15) have obtained a somewhat similar equation and indicate that the distribution should be the same as that for free-free transitions. If one interprets high series as transitions of nearly free electrons, then the plausibility of such an argument is seen.

Even for strong and/or isolated lines, a fully detailed evaluation of Equations (1), (9), and (10) is not required; rather, the line group approximation can be utilized. Initially, the frequency range of interest is divided into a number of increments. Each increment defines as a line group those lines which are centered within it. The line contributions at a frequency point within a frequency increment is obtained by summing over only those lines within its line group. This approximation usually yields a significant simplification with only a negligible loss in accuracy.

2.1.3 Molecular Band Transitions

The rotational lines situated in molecular band systems can also be treated as a pseudo continuum, rather than individually, for many plasma conditions of interest. The density of molecular lines is always very large, and it can be assumed that they are fully overlapped and/or weak. Frequency averaged models are nearly always employed in which only the bands within the system are considered individually (smeared band model) or only the gross shape of the band system itself is retained (bandless model). Such data is adequate for studies in which high spectral resolution is not required.

The low frequency band systems of the air species ($N_2(1+)$, $N_2(2+)$, $N_2^+(1-)$, $O_2(S-R)$, $NO(\beta)$, $NO(\gamma)$) have been extensively studied. Frequency averaged contributions are presented by Aroeste and Magee (Ref. 18) and Biberman and

Mnatsakanyan (Ref. 19), among others. A representative comparison* of their results is given in Figure 2. It is seen that noticeable differences exist in some of the details, but the general levels are in agreement except in the ultraviolet where Biberman and Mnatsakanyan (Ref. 19) included contributions from more transitions. Biberman and Mnatsakanyan (Ref. 19) showed that their data is also in good agreement with the data (viewed with low spectral resolution) of Churchill et.al. (Ref. 20) in which over 150,000 lines were considered individually.

A large number of high frequency band systems have been identified for the air species (see Ref. 21, for example). Sufficient data is not available to allow accurate calculations of the contributions from each individual band system; however, the total contribution from each molecular species can be estimated. Gilmore (Ref. 22) investigated the relative importance of O_2, NO and N_2 in air (contributions from other species being negligible), at $h\nu$ = 9.77 ev and for $2{,}000^\circ K \leq T \leq 8{,}000^\circ K$. He found that O_2, NO and N_2 contributions dominate at low, medium and high temperatures, in that order. The O_2 contribution was attributed to the usual photodissociation continuum. The sources of the NO and N_2 contributions have not been positively identified.

The high frequency contributions of NO were investigated by Biberman and Mnatsakanyan (Ref. 19). They found that the NO(δ) and NO(ϵ) systems make significant contributions in the range 5.2 ev $\leq h\nu \leq$ 8.2 ev and for an extended range of temperature. At higher frequencies, the room temperature data of Watanabe (Ref. 23) show that important contributions from NO exist above $h\nu \approx$ 9.3 ev. Biberman and Mnatsakanyan (Ref. 19) used the room temperature cross sections to estimate the high temperature contribution in this frequency range. The resulting total contribution for NO is high below 8.2 ev and above 9.3 ev with a pronounced minimum in between. This minimum is probably spurious, caused by a lack of data and the use of room temperature cross sections rather than an absence of absorbing mechanisms. Accordingly, Biberman and Mnatsakanyan (Ref. 19) recommend interpolating between the two contributions and disregarding the minimum. In view of the absence of more nearly complete data, this approach seems superior to the usual one of ignoring these systems.

The total high frequency contribution of N_2 has been investigated experimentally by Appleton and Steinberg (Ref. 24) and theoretically by Allen (Ref. 25).** In the experimental study, the contribution in the frequency range

---

* It was necessary to interpolate between the data points presented in Ref. 19 to allow the two sets of data to be compared.

** The contributions of particular band systems have also been studied by Churchill et.al. (Ref. 26) and Gilmore (Ref. 22)

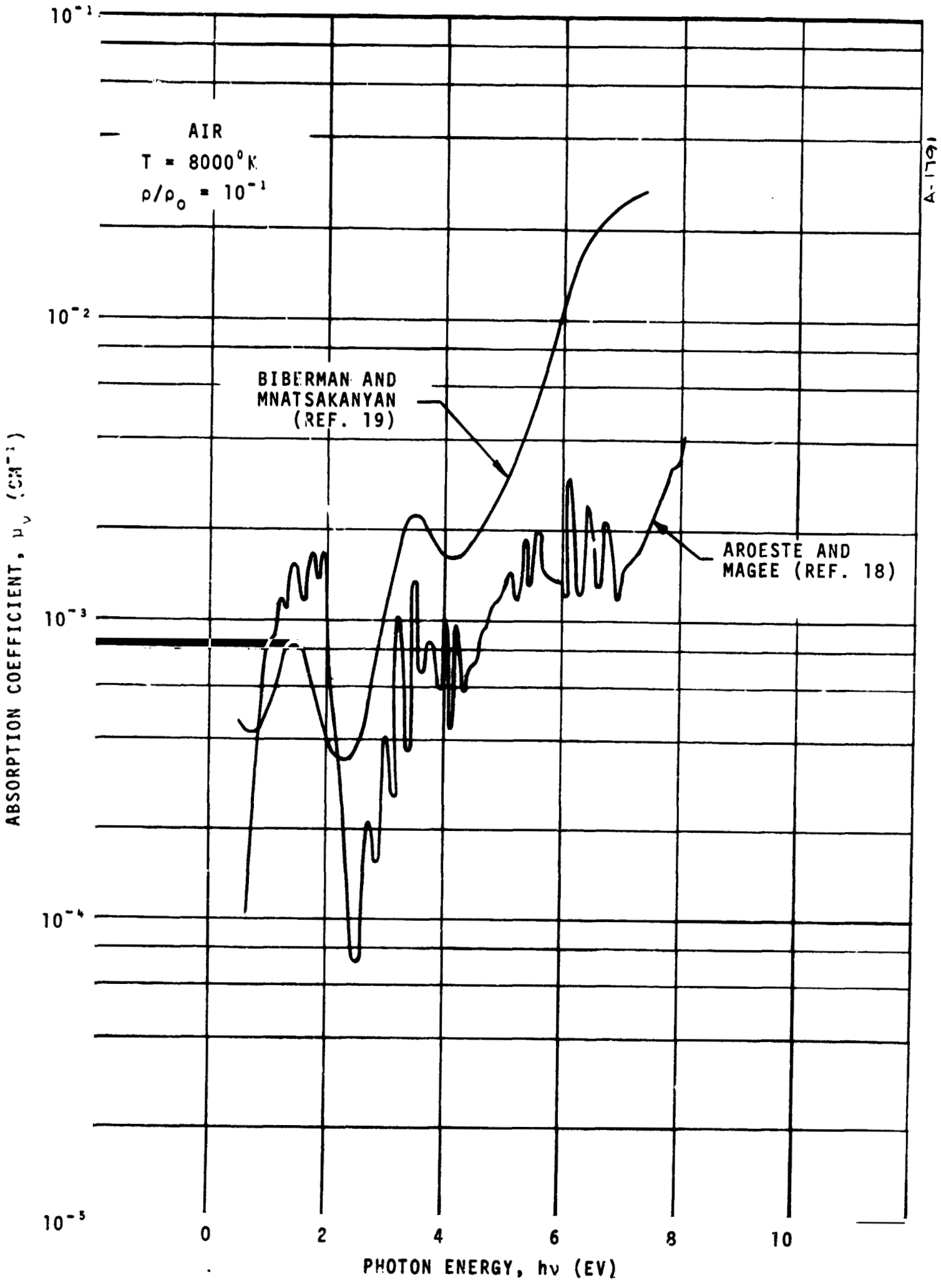

Figure 2. Typical Absorption Coefficient Predictions Including Important Molecular Contributions

9.27 ev ≤ hν ≤ 10.4 ev are measured, and a method is suggested by which they can be obtained to 12.75 ev. In the theoretical study, Allen assumes that the total contribution is dominated by the long wave length "tail" of the N_2 Birge-Hopfield systems $b' \, {}^1\Sigma_u^+ - X \, {}^1\Sigma_g^+$ and $b \, {}^1\Pi_u - X \, {}^1\Sigma_g^+$ for the frequency range 7.0 ev ≤ hν ≤ 14.25 ev. For frequencies above about 10.5 ev, the experimental data is substantially above the calculated data indicating that contributions from sources other than the Birge-Hopfield systems are important. However, there is no reason to believe that Allen's data is in error at the lower frequencies. Thus, the experimental data can be used in the frequency range 9.27 ev ≤ hν ≤ 12.75 ev and the theoretical data in the range 7.0 ev ≤ hν ≤ 9.27 ev.

The contributions from the ablation product species are available from several sources. The species associated with the CO_2 - N_2 system have been studied by Arnold, Reis and Woodward (Ref. 27) and more recently by Woodward (Ref. 28). They considered the CN(V), CN(R), C_2 (Swan) and CO(4+) along with the usual air systems. The contribution from the first three band systems are considered to be reasonably well established. In the case of the CO(4+) system, significantly lower estimates of the magnitude of its contribution are also available (see Ref. 29, for example). The contributions of the C_2 (Freymark), C_2(Fox-Herzberg), C_2(Mulliken), H_2(Lyman) and H_2(Werner) band systems are also available from Weisner (Ref. 30).

2.1.4 Other Transitions

The O_2 Schumann-Runge photodissociation continuum is known to be the most important ultraviolet contributor for the air system at lower temperatures (Ref. 22). Evans and Schexnayder (Ref. 31) have studied this transition experimentally and numerically. A comparison between their results and the approximate Sulzer-Wieland formula

$$\mu_\nu^{PD} = 1.45 \times 10^{-17} \, N_i \left[\tanh\left(\frac{0.0975}{kT}\right)\right]^{1/3} \exp\left[-\tanh\left(\frac{0.0975}{kT}\right)\left(\frac{h\nu - 8.56}{0.805}\right)^2\right] \tag{20}$$

indicates that it is accurate up to temperatures sufficiently high to cause O_2 dissociation, provided that a threshold frequency of 7.1 ev is imposed.

The photodetachment transition of the negative ions of atomic oxygen and hydrogen are known to exist and to be important for some plasma conditions.

The cross sections for O^- are available from the work of Churchill, Armstrong and Mueller (Ref. 26). The cross sections of H^- are very well known and are available from several sources (Refs. 32, 33, and 34), agreement being on the order of five percent. The C^- ion is also known to undergo a photodetachment transition, and cross sections have been obtained by Cooper and Martin (Ref. 35), and are in fair agreement with the measurements of Seman and Branscomb (Ref. 36).

The contribution of the N^- ion is currently being debated. Norman (Ref. 37) argues in favor of an appreciable photodetachment contribution and points out that the utilization of a reasonable cross section ($\sim 8 \times 10^{-17} cm^2$) greatly enhances the agreement between calculated (Ref. 6) and measured (Ref. 38) continuum emission. The recent measurements of Morris et.al. (Ref. 39) also indicates a substantial N^- contribution. However, the N^- contribution is not taken into account in most of the theoretical papers on the emission of an air plasma, including many of the most recent ones (Refs. 5, 10 and 15). It has not been positively established that the ion is stable, especially in its ground state. Further, its photodetachment cross section is completely unknown. Thus, the N^- photodetachment contribution is required to make predictions agree with recent experimental findings, but the transition is not sufficiently well understood to allow predictions to be made from first principles. A numerical investigation of the possible effects of this transition is given in Section 4.1.

The contributions from molecular photoionization transitions are important on occasion. Biberman and Mnatsakanyan (Ref. 19) found that the NO photoionization contribution makes an important contribution to their total high frequency NO contribution. However, other molecules such as CO, H_2, and O_2 have photoionization thresholds at such high frequencies that they can usually be neglected.

Finally, there is reason to believe that absorption and scattering by particulate matter (carbon primarily) can be important for some cases (see Ref. 29, for example). It is felt that this phenomena is not sufficiently well understood to be described quantitatively. Consequently, the present model is applicable to those cases where only a negligible interaction exists between the radiation field and any particulate matter.

2.2 THE RADIATION PROPERTIES MODEL

The radiation properties which are felt to be most nearly consistent with the objectives of the present study are given in Sections 2.2.1, 2.2.2, and 2.2.3. These are ultimately used in the numerical work presented in Section 4.

2.2.1 Molecular Band Model

The bands within each band system are smeared according to the scheme

$$\bar{\mu}_\nu = \frac{\int_{\Delta\nu} \mu_\nu d\nu}{\Delta\nu}$$

where the $\Delta\nu$ are selected such the $\bar{\mu}_\nu$ varies smoothly. The "bandless model" obtained in this fashion is essentially the same as that proposed originally by Meyerott et.al. (Ref. 40) and used more recently by Biberman and Mnatsakanyan (Ref. 19). It is felt to be satisfactory for radiation heating calculations.*

2.2.2 Atomic and Ionic Line Model

The line group approximation is employed to simplify the calculation. The frequency range of interest is divided into a number of frequency increments - 15 to 20 or thereabout. These are not necessarily connected. Each one defines as a line group those lines which are centered within it. The line contributions at a frequency point within a frequency increment is obtained by summing over only those lines within its group.

An additional classification of the lines is required. Lines having a lower level with a principal quantum number (n_L) of four or greater are considered to be high series lines. Contributions from them are obtained from integral formulas (Eq. (19)). Lines having an n_L equal to or less than two are the very strong lines situated in the ultraviolet. The contributions from them are calculated in full detail (within the line group approximation). Lines having an n_L of three appear in the infrared and, to a lesser extent, the visible range of the spectrum. They are of intermediate strength - probably too strong to be calculated by an integral formula but not strong enough to require a fully detailed calculation. Contributions from these lines are obtained by considering the contributions from an "average" line (defined by an averaged line width and f-number) and multiplying by the number of lines. The averaging process is limited to lines within the same line group and having lower levels with the same principal and orbital quantum numbers. This approach neglects line overlapping, an effect which should be of negligible importance for these lines for most cases of interest.

---

*A discussion is given in Section 3.2 on the effect this approximate model has on the calculation of radiative fluxes.

2.2.3 Sources of Data

The mole fractions of the radiating species were calculated using a chemical equilibrium computer program (the ACE program - see Ref. 41). The basic data (specific heats, heats of formation, etc.) were obtained from the compilation of Hochstim (Ref. 42) with some minor modifications to the negative ion data to make them agree better with the recent calculations of Gilmore (Ref. 43). When level populations are required (atomic line and continuum calculations), the appropriate Boltzmann fractions are evaluated as part of the absorption coefficient calculation. The required statistical weights, level energies and partition functions were taken from Gilmore (Refs. 43 and 44).

The radiative properties model adopted for the present calculations was taken from the sources of data given in Tables I-IV. The atomic and ionic continuum contributions are given in Table I, the atomic and ionic lines in Table II, the molecular bands in Table III, and the other contributions in Table IV.

TABLE I

ATOMIC AND IONIC CONTINUUM

Species	Transitions	Source
Hydrogen	High frequency photoionization edges	Eq. (3) with Gaunt factor of unity
	Low frequency photoionization	
	free-free	Eq. (5) with Gaunt factor of unity
Oxygen and Nitrogen	High frequency photoionization edges	Numerical data from Ref. 2
	Low frequency photoionization	Eq. (8) modified empirically to better agree with data from Ref. 2
	free-free	Eq. (5) with Gaunt factor of unity
Carbon	High frequency photoionization edges	Numerical data from Ref. 2
	Low frequency photoionization	
	free-free	Eq. (5) with Gaunt factor of unity
All atomic ions	All transitions	Not included as their continuum transitions are negligibly small

TABLE II

ATOMIC AND IONIC LINES

		Sources of Data			
Species	Transitions	f-no.	Line Shape	$\frac{1}{2}$ width	Other
Hydrogen	Lyman α β Balmer α β	Ref.45	Numerical data from Ref.13	--	Eqs.(13-15) used where applicable
	Other lines accounted for individually	Ref.45	Eq.(10)	Eq.(16)	Eq.(17) used when applicable
	High lines				Ionization threshold lowered ($\tilde{n}$ = 8)
	High series				μ'_ν taken equal to j/B_ν with j from Eq. (19)
Oxygen Nitrogen Carbon (atoms and ions)	All lines accounted for individually	Ref.2	Eq.(10)	Ref.2 and Eq.(11)	Eq.(17) used when applicable
	High lines				Ionization threshold lowered ($\tilde{n}$ = 8)
	High series				μ'_ν taken equal to j/B_ν with j from Eq. (19)

TABLE III

MOLECULAR BAND SYSTEMS

Species	Transitions	Source
N_2	1+ 2+	Curve fits to numerical data from Ref. 19
	Birge Hopfield	Curve fits to numerical data from Ref. 25 for $h\nu \leq 10.5$ ev and from Ref. 24 for $h\nu > 10.5$
O_2	Schumann-Runge Band System	Curve fits to numerical data from Ref. 19
NO	γ β ϵ, δ, photoionization	
N_2	1-	
CN	red violet	Curve fits to numerical data from Ref. 28
C_2	Swan Freymark	Curve fits to numerical data from Ref. 30
	Mulliken	
H_2	Lyman Werner	

TABLE IV

OTHER CONTRIBUTORS

Species	Transitions	Source
O_2	Photodissociation	Eq. (20)
O^-	Photodetachment	Curve fits to numerical data from Ref. 26
H^-	Photodetachment	Curve fits to numerical data from Ref. 32
N^-	Photodetachment	It is not included in the numerical work unless it is called out. Then, the contribution is consistent with the data of Ref. 39
C^-	Photodetachment	Numerical data from Ref. 36
N_2, O_2 CO, H_2 CN, C_2	Photoionization	Neglected
ALL	Particulate absorption and Scattering	Neglected

SECTION 3

TRANSPORT MODEL

3.1 FORMULATION

The basic equation governing the transfer of radiation through a medium in local thermodynamic equilibrium can be written as

$$\frac{dI_\nu}{dS} = \mu'_\nu \left(B_\nu - I_\nu \right) \tag{21}$$

where I_ν is the spectral intensity, B_ν is the Planck function, S is the length of the ray and μ'_ν is the absorption coefficient corrected for induced emission, viz.

$$\mu'_\nu = \mu_\nu \left(1 - \exp\ (h_\nu/kT)\right) \tag{22}$$

and where μ_ν is the ordinary absorption coefficient.

In computing radiation fluxes across boundary and/or shock layers, it is convenient to make the tangent slab approximation. Thus, the properties along any ray can be related to those along the normal coordinate (y) by applying a cosine transformation. The coordinate system is shown in Figure 3. The resulting expressions for the optical depth, spectral fluxes and total flux are well known and can be written in the form

$$\tau_\nu = \int_o^y \mu'_\nu dy \tag{23}$$

$$F^+_\nu(y) = \int_o^{\epsilon^+_b} E_\nu(\epsilon^+_\nu)\, d\epsilon^+_\nu \tag{24}$$

$$F^-_\nu(y) = -\int_o^{\epsilon^-_b} E_\nu(\epsilon^-_\nu)\, d\epsilon^-_\nu \tag{25}$$

$$q_r(y) = \int_o^\infty \left[F^+_\nu(y) - F^-_\nu(y) \right] d\nu \tag{26}$$

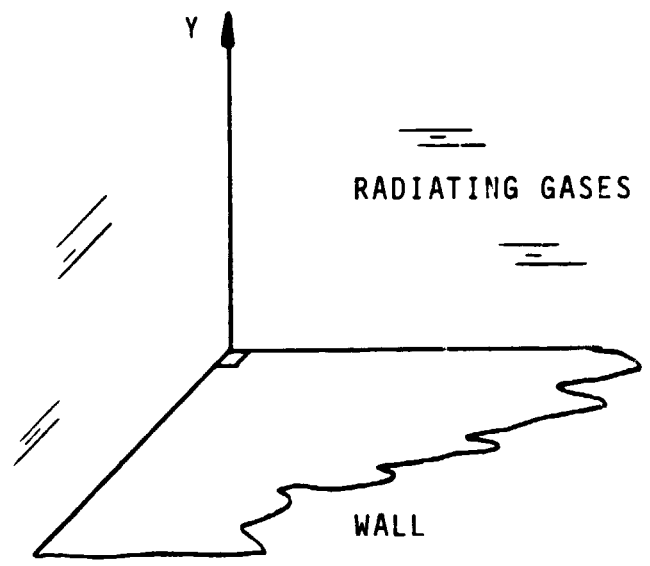

Figure 3. Coordinate System

where fluxes entering or reflected at y = 0 have been neglected (a cold, black wall is assumed). The quantity E_ν is the black body emissive power defined as

$$E_\nu = \pi B_\nu \tag{27}$$

Finally, Equations (23) and (24) utilize emissivities as independent variables where

$$\epsilon_\nu^+ = 1 - 2\mathscr{E}_3(t_\nu - \tau_\nu) \tag{28}$$

$$\epsilon_\nu^- = 1 - 2\mathscr{E}_3(\tau_\nu - t_\nu) \tag{29}$$

and the $\mathscr{E}_n(x)$ functions are exponential integrals of order n.

The exponential approximation can be used to further simplify the equations without an appreciable loss in accuracy. It is known (see Ref. 15, for example) that when the approximation

$$2\mathscr{E}_3(x) \approx \exp(-2x) \tag{30}$$

is made, exact transport solutions are obtained in the optically thin and optically thick limits, and good approximations are obtained at intermediate optical depths. Thus, the emissivities become

$$\epsilon_\nu^+ \approx 1 - \exp 2(\tau_\nu - t_\nu) \tag{31}$$

$$\epsilon_\nu^- \approx 1 - \exp 2(t_\nu - \tau_\nu) \tag{32}$$

which are more convenient to work with than those given by Equations (28) and (29). Emissivities written in this form have the additional advantage that by suppressing the factor of 2 in the exponential arguments and replacing E_ν by B_ν in Equations (23) and (24), the same formulation can be used to calculate intensities.

Before evaluating Equations (23)-(26) it is advantageous to separate the integrals into line and continuum parts. This allows optimum coordinates to be selected in frequency space. The continuum contribution to the absorption

coefficient ($\equiv \mu_\nu^C$) is just the first term in Equation (1). Substituting μ_ν^C for μ_ν in Equations (23)-(26) yields corresponding values for τ_ν^C and F_ν^C, where the $\pm$ signs have been dropped from the latter for brevity. The line contributions to the flux are obtained by difference

$$F_\nu^L \equiv F_\nu - F_\nu^C \tag{33}$$

where the F_ν values are evaluated using the total absorption coefficient (Eq. (1). Thus, the line contribution is treated as a correction to the continuum flux.*

3.2 EVALUATION OF FLUX INTEGRALS

A direct evaluation of Equations (23)-(26) requires an implicit assumption - that only a reasonable number of frequency points need be sleected to adequately describe the variation of the spectrum. In the case of the continuum spectrum, the assumption is well satisfied with about 25-50 points being sufficient. In the case of atomic lines, the number is approximately 1,000 frequency points (100 lines with 10 points per line), which is getting large but can still be handled for most cases. In the case of molecular lines the requirement rises to approximately 1,500,000 frequency points (150,000 lines with 10 points per line), which is quite impractical for radiation heating calculations.

In the present study, the problem of resolving the molecular spectrum is solved summarily. The utilization of the molecular band model (the bandless model) converts the molecular spectrum into an "equivalent" continuum process. Such an approach ignores the details of the internal structure of the band system. The calculated spectral fluxes yield the correct total fluxes (when integrated over a band system) only when the layer is optically thin, optically thick, or when the lines are spaced sufficiently close together to

*It should be noted that the line contributions defined by Equation (33) can be negative for nonisothermal layers.

be strongly overlapped. Otherwise, only an approximation to the total flux is obtained.*

No additional approximations are required. The continuum fluxes and the approximation to the molecular line fluxes can be calculated in a straightforward manner. The atomic and ionic line fluxes can also be obtained directly. While thi. calculation is lengthy, it is not felt to be excessively so. In all cases careful attention must be paid to the selection of nodal points (in frequency and in space) and interpolation formulas to insure that high accuracy is maintained.

3.2.1 Nodal Points in Frequency

For the continuum contribution to the flux integrals the frequency grid can be specified a priori and is only slightly dependent on the characteristics of the layer. Basically, the variation of the Planck function and the continuum absorption coefficients must be adequately described. The first requirement can be met by distributing nodal points across the frequency range $h\nu \approx 0.25$ ev to $h\nu_{max} \approx 12\ kT_{\infty}$ ev. Usually about 30 points spaced at roughly equal intervals are sufficient. This grid also satisfies the second requirement except in the ultraviolet. There the frequency grid must be carefully selected to resolve the photoionization thresholds.**

---

* The accuracy of the approach can be defended on the following grounds: (1) The molecular spectra for which good property data are available are all situated in the infrared, visible, or near ultraviolet. It is well known that this region of the spectrum is optically thin for typical boundary or shock layer conditions and, hence, the bandless model is accurate for these data. (2) The molecular spectra situated in the ultraviolet and the vacuum ultraviolet are often strong enough to absorb appreciably. However, good radiation property data are not available in this region; consequently, the bandless model approach is consistent with the quality of the data. (3) Finally, and of primary importance, it is known that whenever radiation heating is comparable to convective heating, the molecular species will be confined to a narrow layer near the wall. The radiation will originate in the external region of the flow which will be hot enought to be dissociated and at least partially ionized. Thus, in any competition for accuracy and/or detail the atom and ion radiation must be given preferential treatment.

It is to be noted that more sophisticated band models are used by some investigators. These extend the range of validity somewhat, but introduce what is basically the same type of approximation and are accurate in the same regimes.

** It should be noted that the movement of the thresholds (in frequency) caused by plasma interaction effects is not considered. This is consistent with the approximation discussed in Section 2.

For the line contribution to the transport integrals, a grid must be selected for each line and should be dependent upon the characteristics of the layer as well as the individual line. This is accomplished by introducing a parameter φ which is characteristic of the width of the line (and will be discussed further in a subsequent paragraph) to stretch the coordinate system. The smallest increment and the distance to the most remost nodal point are defined by Equations (34) and (35), respectively, where $\tilde{\nu} = |\nu - \nu_c|$.

$$\delta\tilde{\nu}_o = f_1\varphi \tag{34}$$

$$\tilde{\nu}_{max} = f_2\varphi \tag{35}$$

The quantities f_1 and f_2 are selected arbitrarily and are usually taken to be 0.5 and 10 (respectively), on this order. The intermediate nodal points are established using a growth law, viz.

$$\delta\tilde{\nu}_j = (1 + f)\ \delta\tilde{\nu}_{j-1} \tag{36}$$

where the nodal spacing increases (increasing subscript j) with increasing distance from the center of the line. The growth factor f is determined implicitly from the relation

$$\tilde{\nu}_{max} = \frac{(1 - f)^N - 1}{f}\ \delta\tilde{\nu}_o \tag{37}$$

where N is the number of increments to be used. Usually, the center of the line and about 5 to 7 additional points in each direction from it are sufficient.

The stretching parameter φ is defined by Equation (38),

$$\varphi \equiv \gamma(\bar{y})\sqrt{1 + \tau_c} \tag{38}$$

where the (half) half width $\gamma(\bar{y})$ is evaluated at a particular spatial location (usually as an edge condition) and τ_c is the optical depth of the entire layer at the frequency of the center of the line. It can be shown that φ has the following properties:

$$\lim_{\tau_c \to 0} \varphi = \gamma(y) \tag{39}$$

$$\lim_{\gamma/h\tilde{\nu} \to 0} \varphi \approx h\nu \Big|_{\tau_{\tilde{\nu}} = 1} \tag{40}$$

That is, the φ is the distance in frequency space from the center of the line to the half intensity position when the line is weak, and it is approximately the distance to the frequency at which the layer has unit optical depth when the line is strong. At intermediate values of τ_c, φ should also be a reasonable approximation to the width of the line.

3.2.2 Nodal Points in Space

Initially a spatial grid is selected so that it adequately describes the variations of the thermodynamic properties across the radiating layer (the circles shown in Figure 4, for example). The optical depths are then calculated* and used to evaluate the emissivities. Typical values are shown in Figure 4(b) where Curves 1, 2 and 3 illustrate the optically thin, moderately thick and very thick layers, respectively. Transforming into the E_ν vs. ϵ_ν plane yields the points shown (as circles) in Figure 4(c). Curves 1 and 2 are well-behaved; however, Curve 3 is very ill behaved, showing essentially a singularity at the outer boundary. To circumvent the problems caused by this

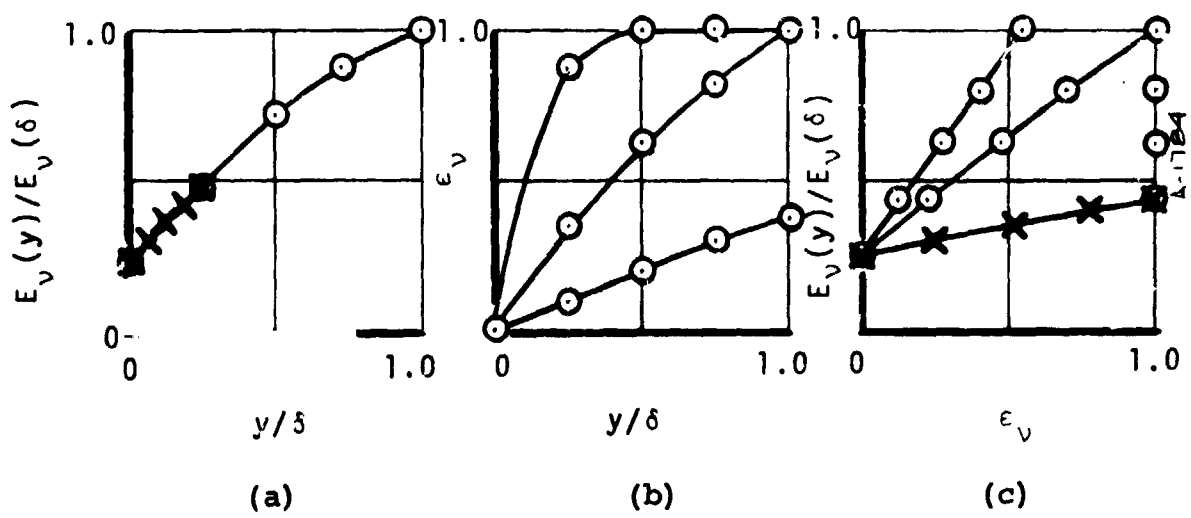

Figure 4. Spatial Grid Transformations

*The methods used to evaluate the integrals appearing in Equations (23)-(26) will be described subsequently.

behavior, a special coordinate system is used for the optically thick layers ($\tau_\nu > 2$ for present purposes). The layer is divided into equal increments of emissivities (crosses in Figure 4(c) from which the new values of optical depth are calculated.* The new E_ν values are then obtained by cubic interpolation in the plane $\ln E_\nu$ vs. $\ln \tau_\nu$.** The new curve in the E_ν vs. ϵ_ν plane (crosses in Figure 4(c)) is suitable for accurate evaluation by numerical methods.

3.2.3 Integration Scheme

With one exception, all the integrals are evaluated using three term Taylor's series expansions as interpolation formulas. The derivatives required in the second two terms are obtained from Equation (41), where x and y are the general independent and dependent variables, respectively.

$$\frac{dy}{dx} = ys \tag{41}$$

The s values are taken equal to the slopes in the plane ln y vs. x and are obtained from curve fits. It has been found that this procedure minimizes unwanted excursions in the higher order terms.

The Taylor's series expansions cannot be used for the frequency integration of the continuum fluxes due to the discontinuities in the integrals. These integrals were evaluated using linear interpolation formulas, instead. This causes no serious loss in accuracy as the integrals are slowly varying except at the discontinuities.

3.3 THE RADIATION TRANSPORT PROGRAM (RAD)

The entire solution procedure has been programmed for the Philco 212 and Univac 1108 computers. A description of the code has been presented elsewhere (Ref. 46). Typically, about 30 seconds of Univac 1108 computer time are required to calculate the flux from the boundary of a uniform layer. The calculation of the flux distribution across a layer containing a C-H-O-N elemental mixture requires slightly more than 1 minute.

---

*In evaluating the optical depths, the maximum allowable value of ϵ_ν is taken to be 0.99.

**The origin of the optical depth integration is shifted and/or inverted in space to insure that the $\ln E_\nu$ vs. $\ln \tau_\nu$ curve is well behaved for the interpolation.

SECTION 4

APPLICATION OF THE METHOD

A matrix of theoretical predictions has been obtained. Selected cases are compared with predictions from other studies in Section 4.1 and with experimental data in Section 4.2. Calculations of the radiative transport through isothermal layers are given in Section 4.3 and through a noniosthermal layer in Section 4.4, both as examples of the use of the prediction method.

4.1 COMPARISON WITH OTHER PREDICTIONS

The first set of theoretical predictions is given in Figure 5 and compared with the semi-empirical predictions of Morris et.al. (Ref. 39). Three predictions are presented using the present model - one without an N^- contribution, one with an N^- contribution and a cross section of 8×10^{-17} cm^2 as suggested by Norman (Ref. 37), and one with an N^- contribution and a cross section of 1.6×10^{-16}cm^2 which makes the present predictions agree with the predictions of Morris et.al. (Ref. 39). While a cross section of 1.6×10^{-16} cm^2 is larger than that of most continuum transitions, it is neither so large nor so different from the one suggested by Norman (Ref. 37) as to appear to be unreasonable. However, based on this evidence alone, it cannot be concluded that the present predictions are consistent with those of Morris et.al. (Ref. 39).

Additional predictions of the nitrogen continuum intensities are given in Figure 6 and compared with the predictions of Biberman and Norman (Ref. 6) and with the data of Boldt (Ref. 38) and Morris et.al. (Ref. 39). It is seen that the present predictions (without N^-) are greater than those by Biberman and Norman (Ref. 6) by about a factor of two;* likewise, the measurements of Morris et.al (Ref. 39) are greater than the measurements of Boldt et.al. (Ref. 38) by about a factor of two. Thus, assigning the difference between measurement and prediction to the N^- contribution can yield either the rough agreement noted previously or gross differences in the N^- cross section, depending on the combinations of measurements and predictions selected. It is also seen in Figure 6 that the present predictions (without N^-) are in fair agreement with both sets of measurements and that the slopes of all the predictions

*In this spectral region, the absorption coefficients used by Biberman and Norman (Ref. 6) dip below those used in the present study; otherwise, the agreement is generally very good.

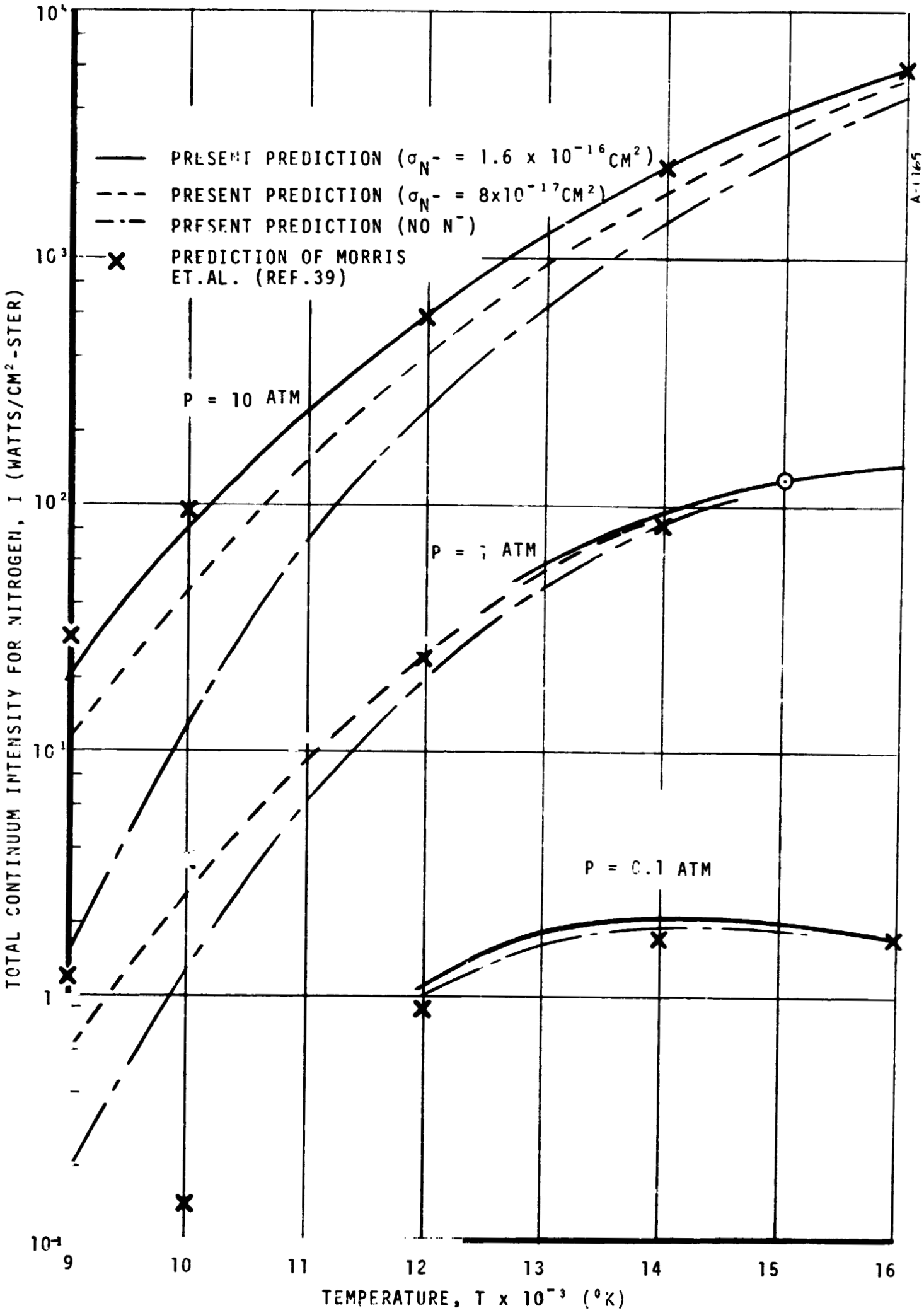

Figure 5. Comparison with the Predictions of Morris et.al. (Ref. 39)

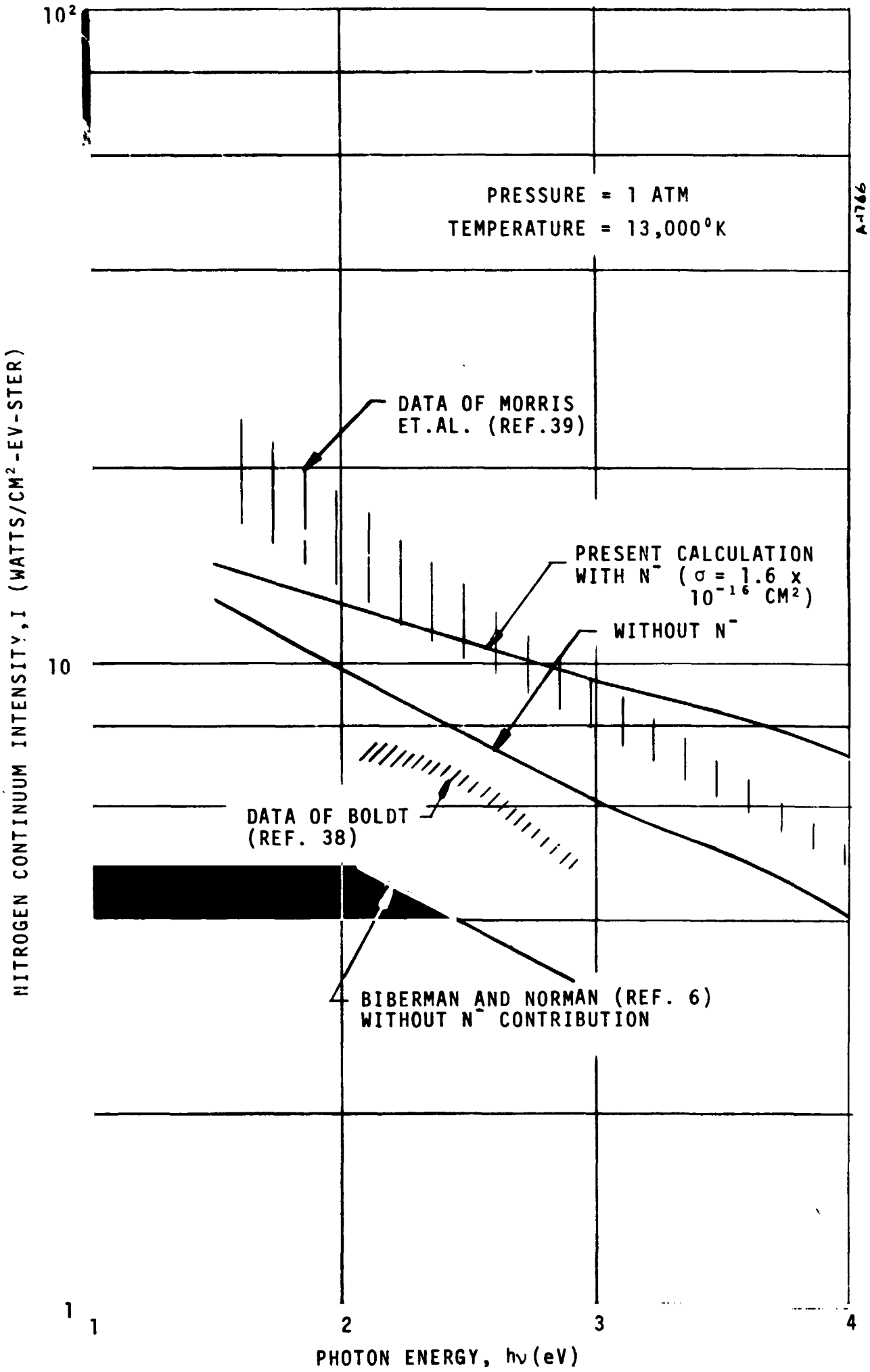

Figure 6. Effect of N^- on the Spectral Distribution of the Intensity of Nitrogen, δ = 1 cm

(without N^-) are in good agreement. The agreement in slope is destroyed when the N^- contribution is included in the present predictions.* Thus, forcing agreement between the present predictions and the total intensitites predicted by Morris et.al. (Ref. 39) decreases the agreement between the predictions and their spectral data. Thus, it can be concluded that the present predictions (without N^-) are in fair agreement with the predictions and measurements of Morris et.al. (Ref. 39) and that the inclusion of an N^- increases only certain aspects of this agreement. The numerical work to be presented subsequently does not contai an N^- contribution unless it is specifically called out.

The theoretical predictions for air are presented in Figure 7 and compared with the theoretical predictions of Wilson and Greif (Ref. 10). Their properties model for the atomic and (positive) ionic species is very similar to that used in the present study (Ref. 2). However, they did not include contributions from the molecular species or the negative ions. In addition, they employ the effective width approach which approximates the contributions due to the atomic and ionic lines. The resulting predictions (Fig. 7) are in excellent agreement for the δ = 1 cm case except at the lower temperatures where the molecular contributions are clearly important. For the δ = 10 cm case, the predictions differ by about 25 - 35 percent, even in the temperature range where no differences should exist. This difference cannot be attributed to fundamental differences in either the properties or the transport models. Molecular contributions are negligible above about $T \approx 12{,}000^{\circ}K$. In addition, the differences in calculating line effects cannot be responsible as they would be in the opposite direction. However, Wilson and Greif (Ref. 10) utilize Equation (8) as a convenient approximation to the continuum absorption coefficients, rather than the numerical data presented in Reference 2. While the agreement between the two is generally very good (see Fig. 1), an error exists in the 1.5 - 4 ev range which is sufficient to cause the differences observed.

A comparison with the theoretical predictions of air by Biberman et.al. (Refs. 8 and 19) is given in Figure 8. The differences between their property data and that used in the present study are not large for the line radiation, both f - numbers and line widths being in good agreement. Further, the properties used for the molecular species contributions are from the same source

*If the N^- cross section were assigned a variation in frequency, agreement with the spectral data of Morris et.al. (Ref. 39) could be maintained; however, there presently exists no basis for such an assignment.

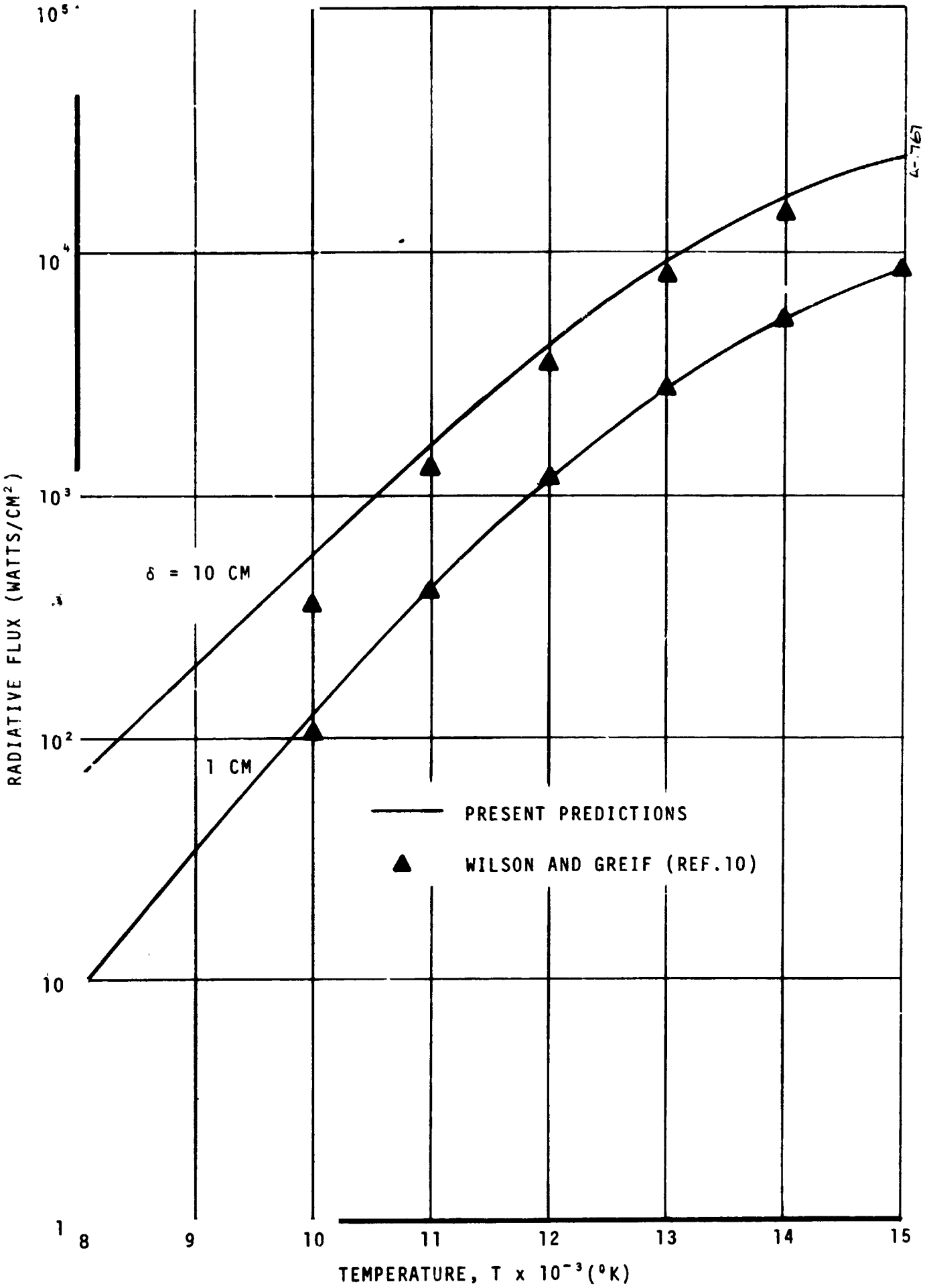

Figure 7. Flux Emitted from a Uniform Air Slab, P = 1 atm

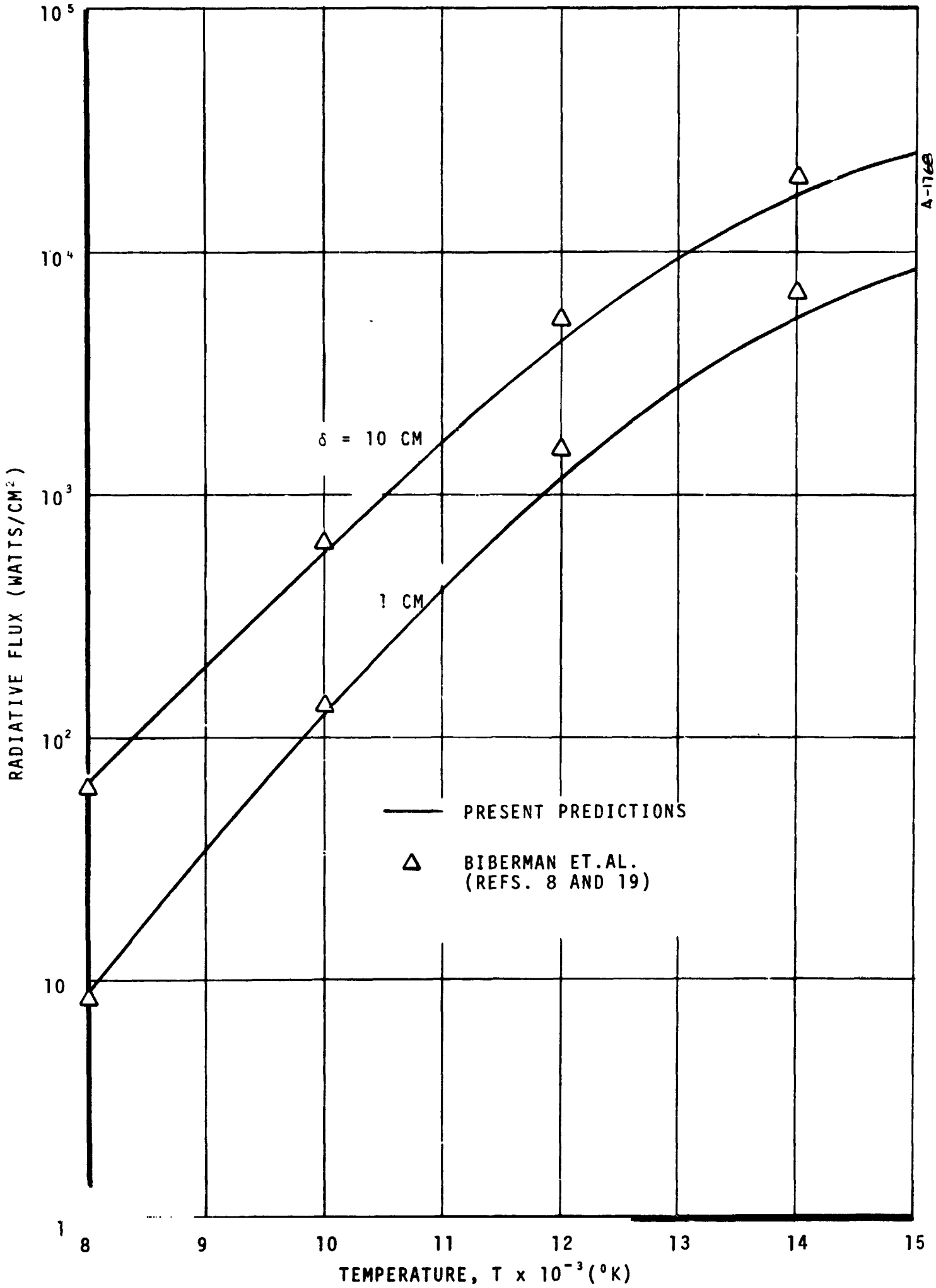

Figure 8. Flux Emitted from a Uniform Air Slab, P = 1 atm

(Ref. 19). The differences are slightly more appreciable in the case of the continuum radiation properties. They use Equation (8) and include a contribution from the N^- ion. The addition of the N^- continuum in the 1.5 ev to 4 ev spectral region more than compensates (usually) for the differences between Equation (8) and the data given in Reference 2. Thus, the fluxes Biberman et.al. (Refs. 8 and 19) predicts are consistently higher than those predicted in the present study. However, reference to Figure 8 indicates that the differences are not large.

A comparison with the theoretical predictions of Hunt and Sibulkin (Ref. 15) for pure nitrogen is given in Figure 9. They obtained their molecular species contributions from Allen (Ref. 47), their continuum radiation from the tabulations of Sherman and Kulander (Ref. 48), their f-numbers from Kelly (Ref. 49) and their half widths from Griem (Ref. 9). The tabulations of Sherman and Kulander (Ref. 48) are somewhat higher than those used in the present study (Ref. 2). None of the data obtained from the other sources is significantly different from that used in the present study. Hunt and Sibulkin do handle the transport slightly differently in that J-splitting is considered and quasi-static line profiles are used for some of the higher lines. However, reference to Figure 9 indicates that these differences are not significant as good agreement exists between the two sets of predictions.

A comparison with the theoretical predictions of Lasher et.al. (Ref. 3) for hydrogen is given in Figure 10. The classical formulas for f-numbers and continuum absorption coefficients were used in both studies. However, Lasher et.al. (Ref. 3) utilize somewhat different line shapes (Eqs. (13)-(15). only), and they employ the equivalent width approximation. In addition, Lasher et.al. (Ref. 3) are concerned only with the atomic contributions and do not include contributions from molecular or ionized species. As shown in Figure 10, their model is not applicable at ten atmospheres for the lower temperatures. However, the two sets of predictions are in good agreement at the low r pressures.

4.2 COMPARISONS WITH MEASURED DATA

Predictions of the emission coefficients of shock heated air are given in Figures 11, 12 and 13 and compared with the measurements of Nerem (Ref. 50) and Gruszczynski and Warren (Ref. 51). The predictions are in excellent agreement with the data of Nerem (Ref. 50), but they are somewhat lower than the data of Gruszczynski and Warren (Ref. 51). The basic techniques used in the

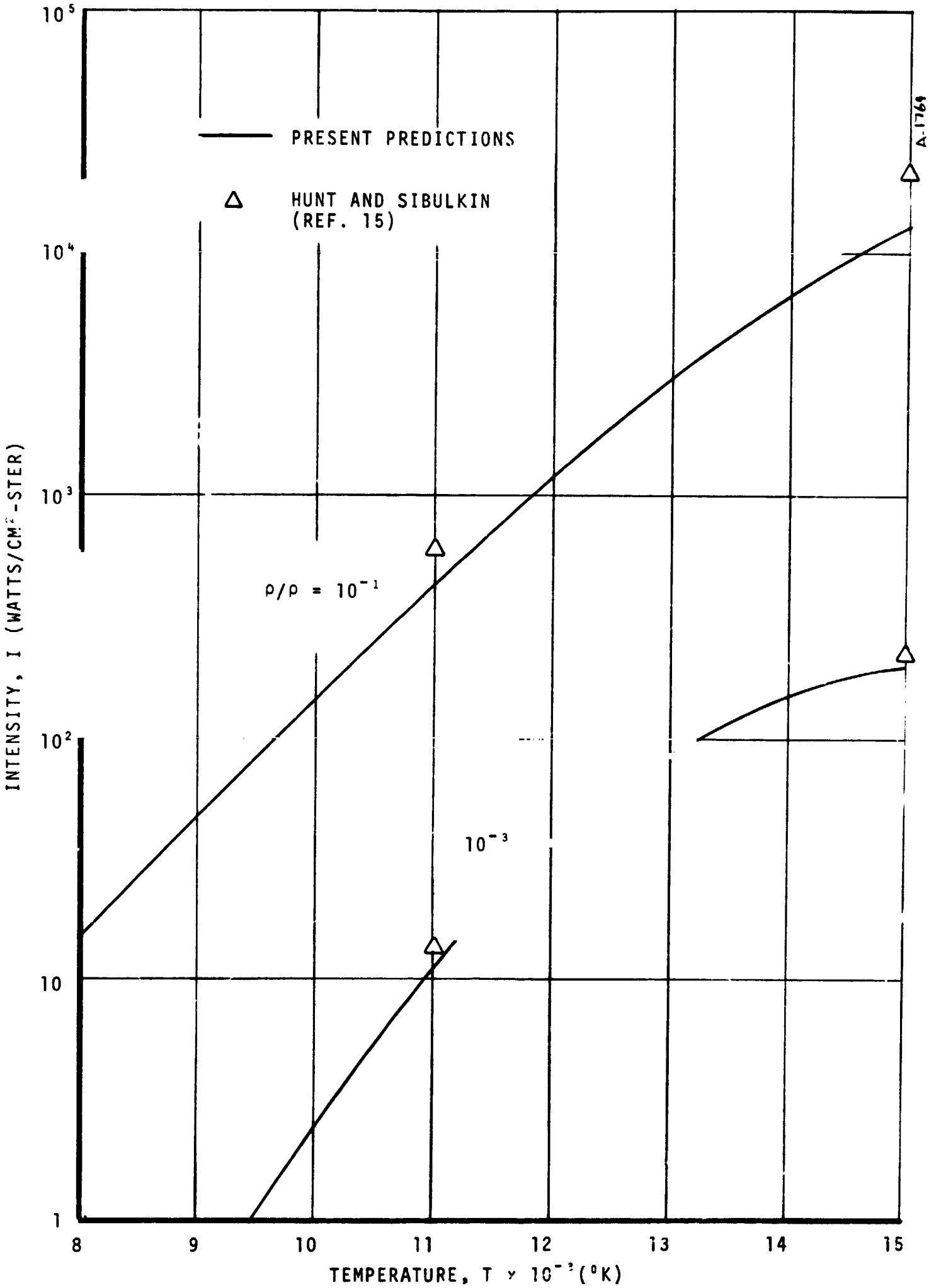

Figure 9. Intensity Emitted from a Uniform Nitrogen Slab, δ = 1 cm

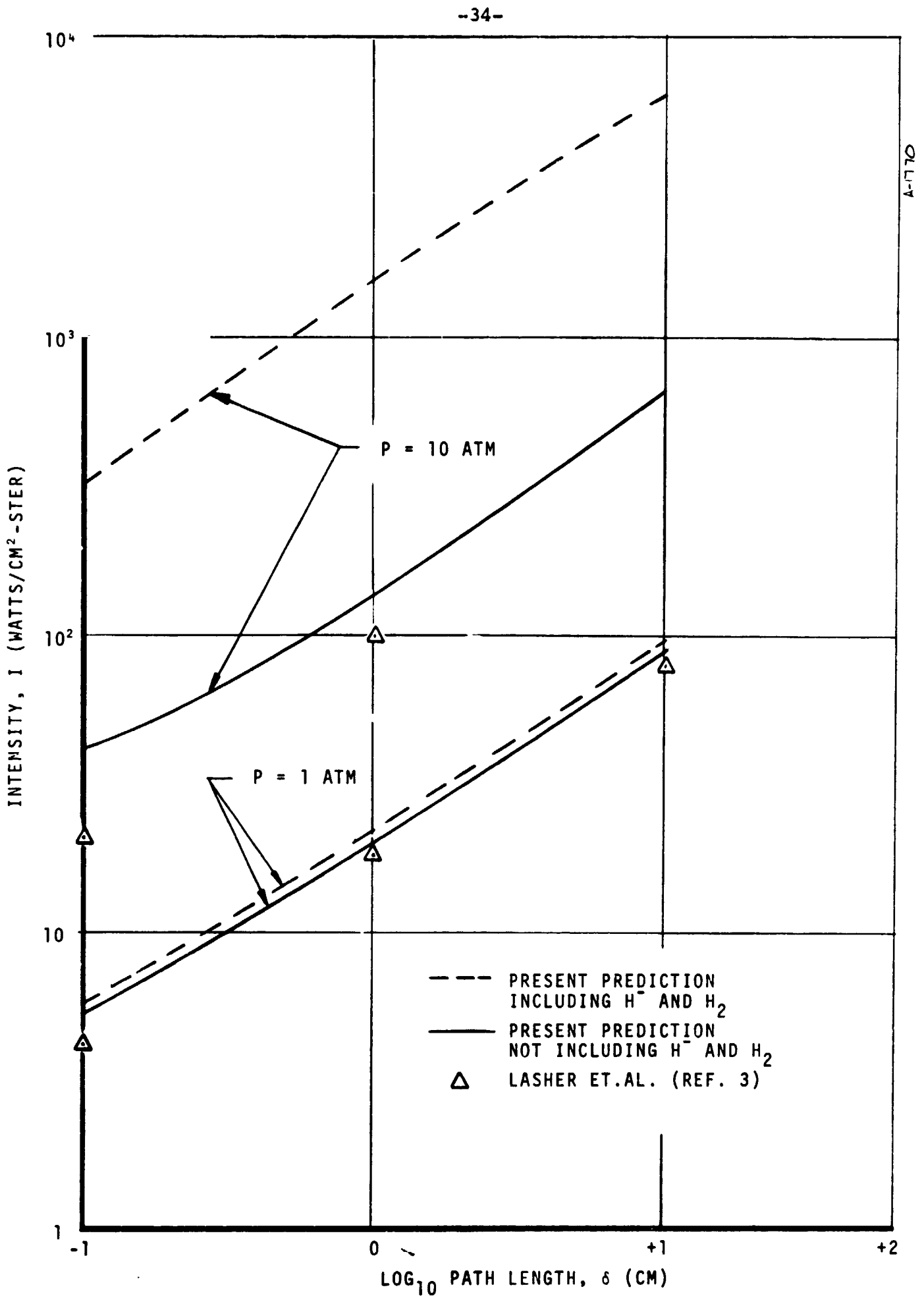

Figure 10. Intensity Emitted from a Uniform Hydrogen Slab, T = 10,000°K

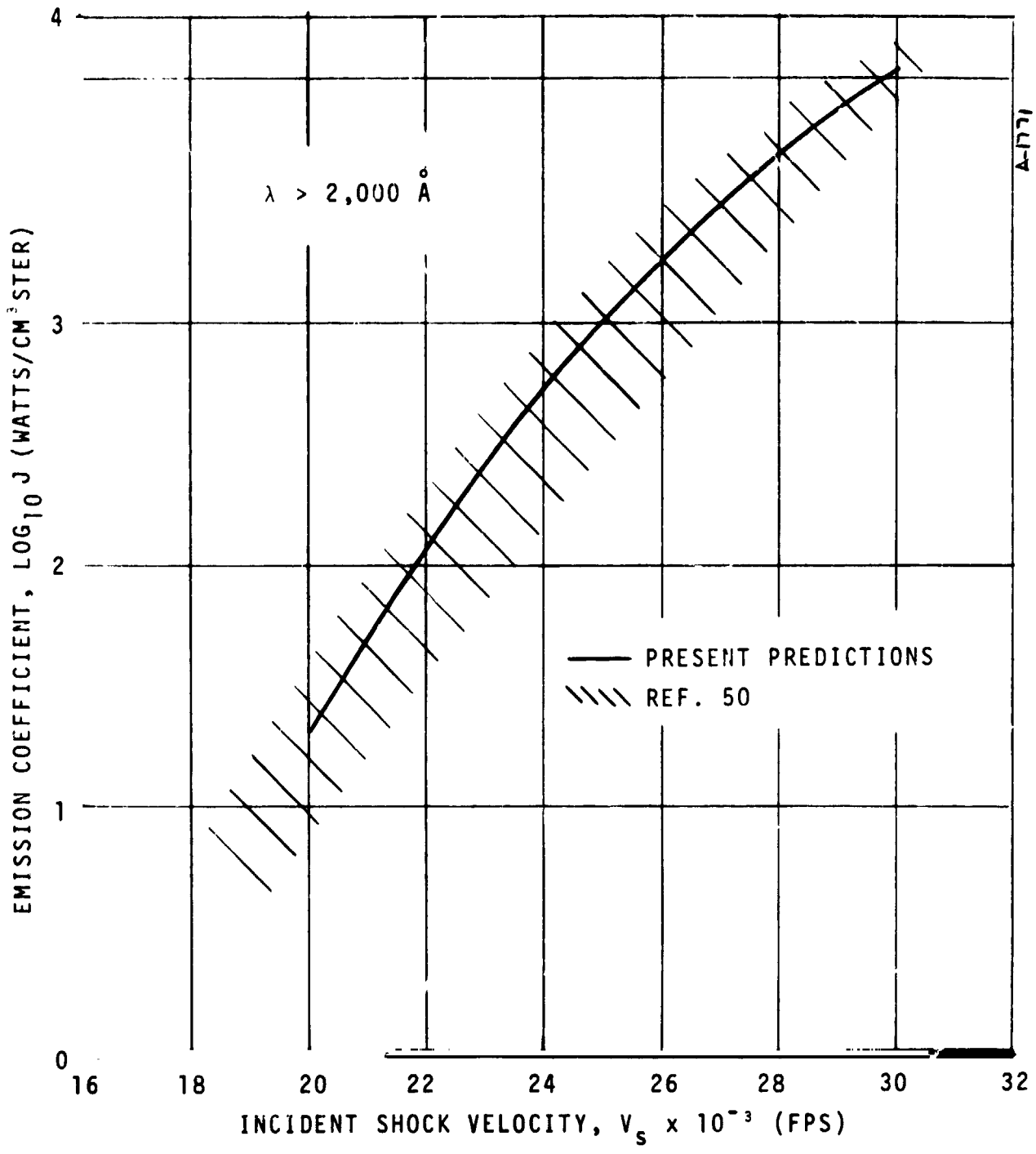

Figure 11. Comparison with the Shock Tube Data of Nerem (Ref. 50), P_1 = 1 mm Hg

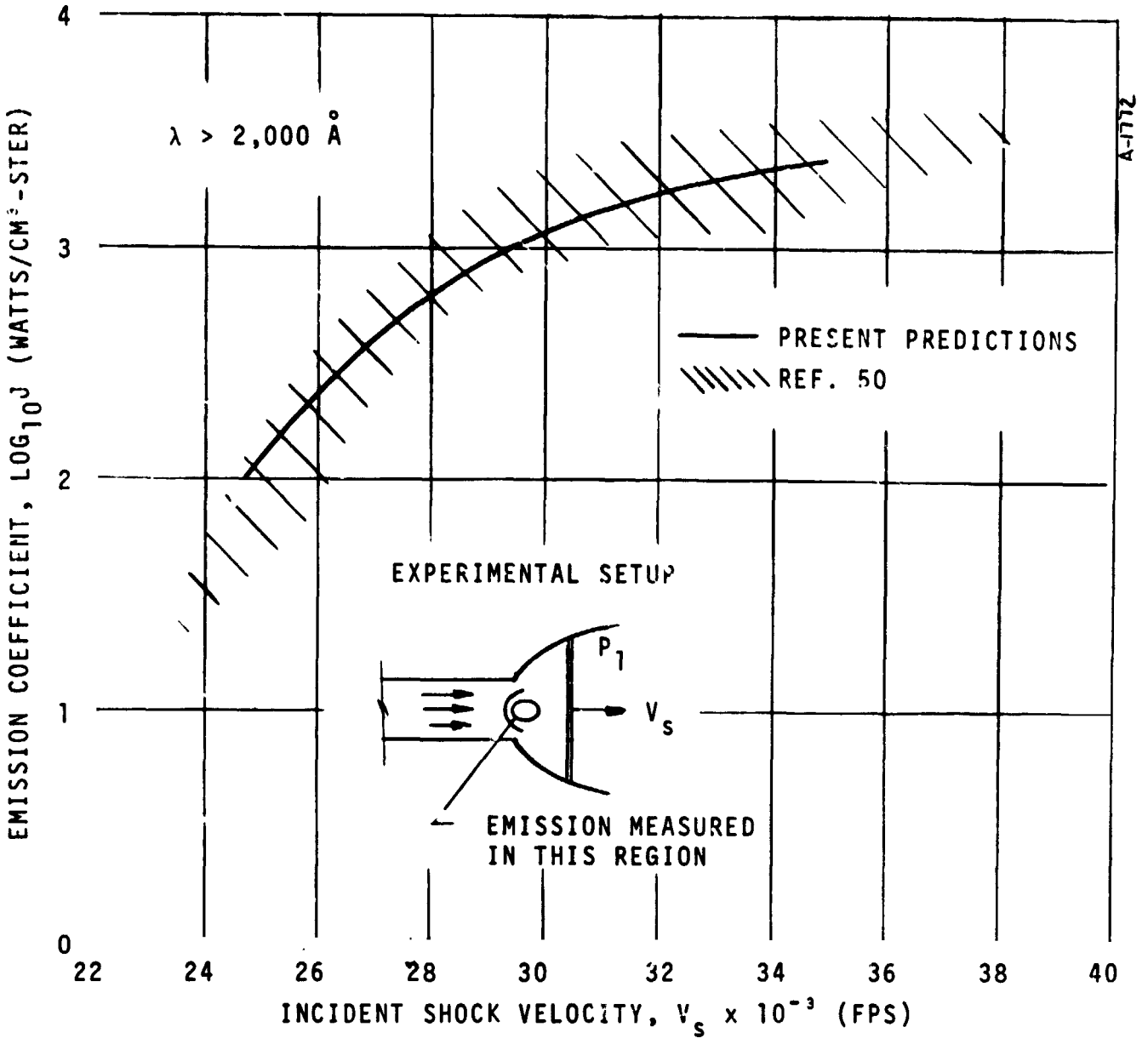

Figure 12. Comparison with the Shock Tube Data of Nerem (Ref. 50), P_1 = 2 mm Hg

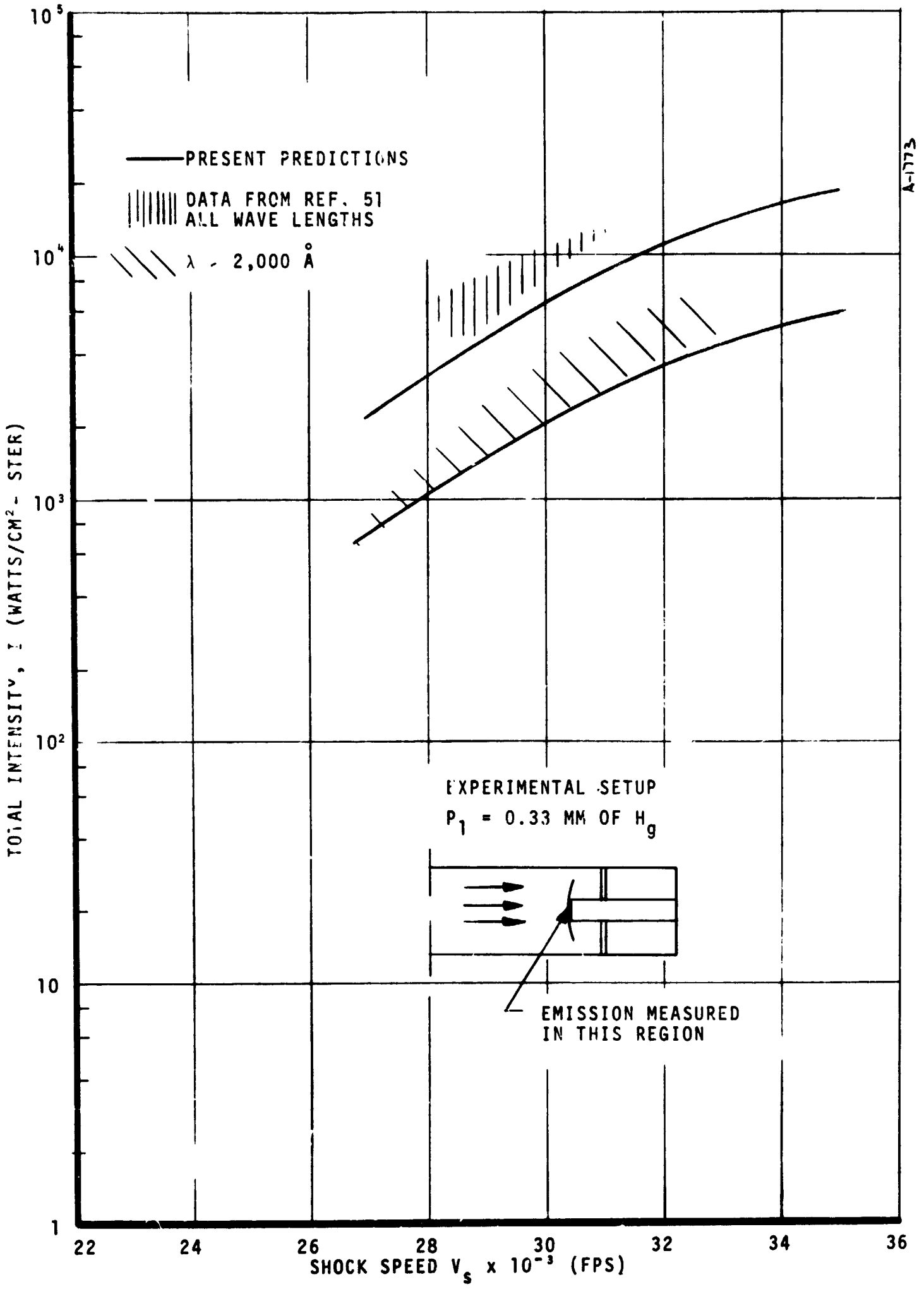

Figure 13. Comparison with Shock Tube Data of Kuszynski and Warren (Ref. 51)

two experimental studies are very similar, and the same general range of conditions were covered. It is unfortunate that the two sets of results are not in better agreement with each other. Nevertheless, the general agreement between prediction and experiment is felt to be encouraging.

The predicted intensities of air behind a reflected shock wave are given in Figures 14 and 15 and compared with the measurements of Wood et.al. (Ref. 52) as revised and supplied by Wood (Ref. 53). The predictions are in excellent agreement with the measurements for incident shock velocities less than 7.5 mm/μ sec. and are above the measurements at higher velocities. Golobic and Nerem (Ref. 54) have analyzed a reflected shock experiment similar to that performed by Wood et.al. (Ref. 52) and have concluded that the radiation losses significantly cool the gases for incident shock velocities above 7.5 mm/μ sec. They present calculated intensities for the low frequency spectrum ($\lambda > 1{,}700$ Å) showing the effect of the losses. Obtaining their predicted ratios of intensities with radiation losses to those without losses (as a function of incident shock velocity) and using them to (approximately) correct the prediction given in Figure 14 yields the dashed curve and a dramatically improved comparison between prediction and measurement. Such an effect would obviously affect the total intensities also. Thus, the present predictions appear to agree w. . the data of Wood (Ref. 53).

This concludes the series of comparisons with the wor': of other investigators. It is felt that the model has been proven to be a valid one. Subsequent numerical work will be used to illustrate interesting applications.

4.3 APPLICATION TO UNIFORM SLABS

Theoretical predictions for uniform slabs are given in Figures 16 and 17. They show the variation of the fluxes emitted from uniform slabs of air. The ranges of temperature, pressure and path lengths selected are typical of those which might be encountered in the stagnation region of a vehicle reentering from a lunar or planetary mission.

4.4 APPLICATION OF NONUNIFORM SLABS

To further illustrate applications of the method, a slab with nonuniform properties was selected and its distributions of flux in space and frequency obtained. The variations of the thermodynamic state properties across the slab are given in Figure 18 where the overall length of the slab (y_δ) is 11.4 cm. This variation is typical of that which might be found in the stagnation region

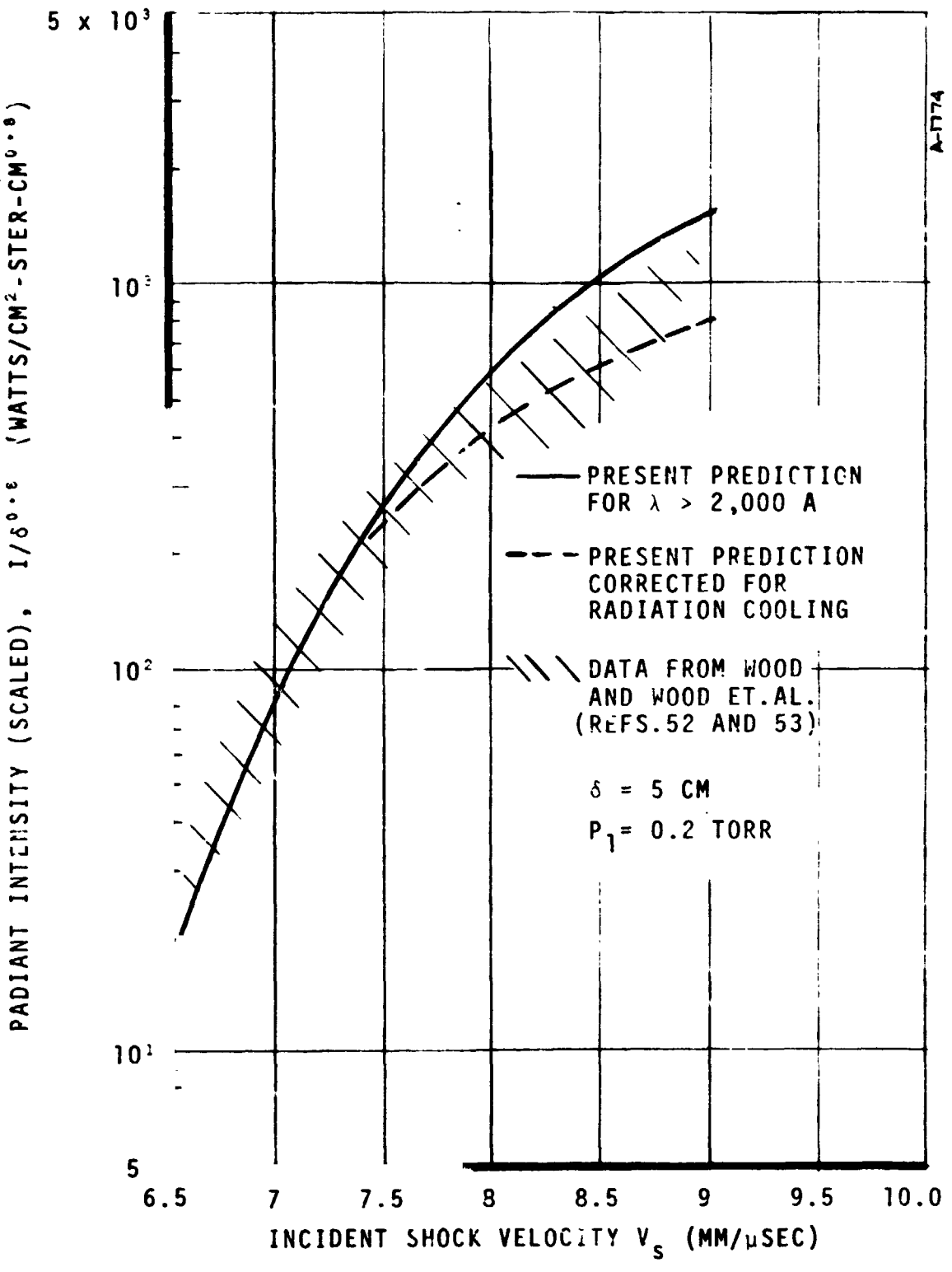

Figure 14. Comparison with Shock Tube Data of Wood (Ref. 53) and Wood et.al.(Ref. 52)

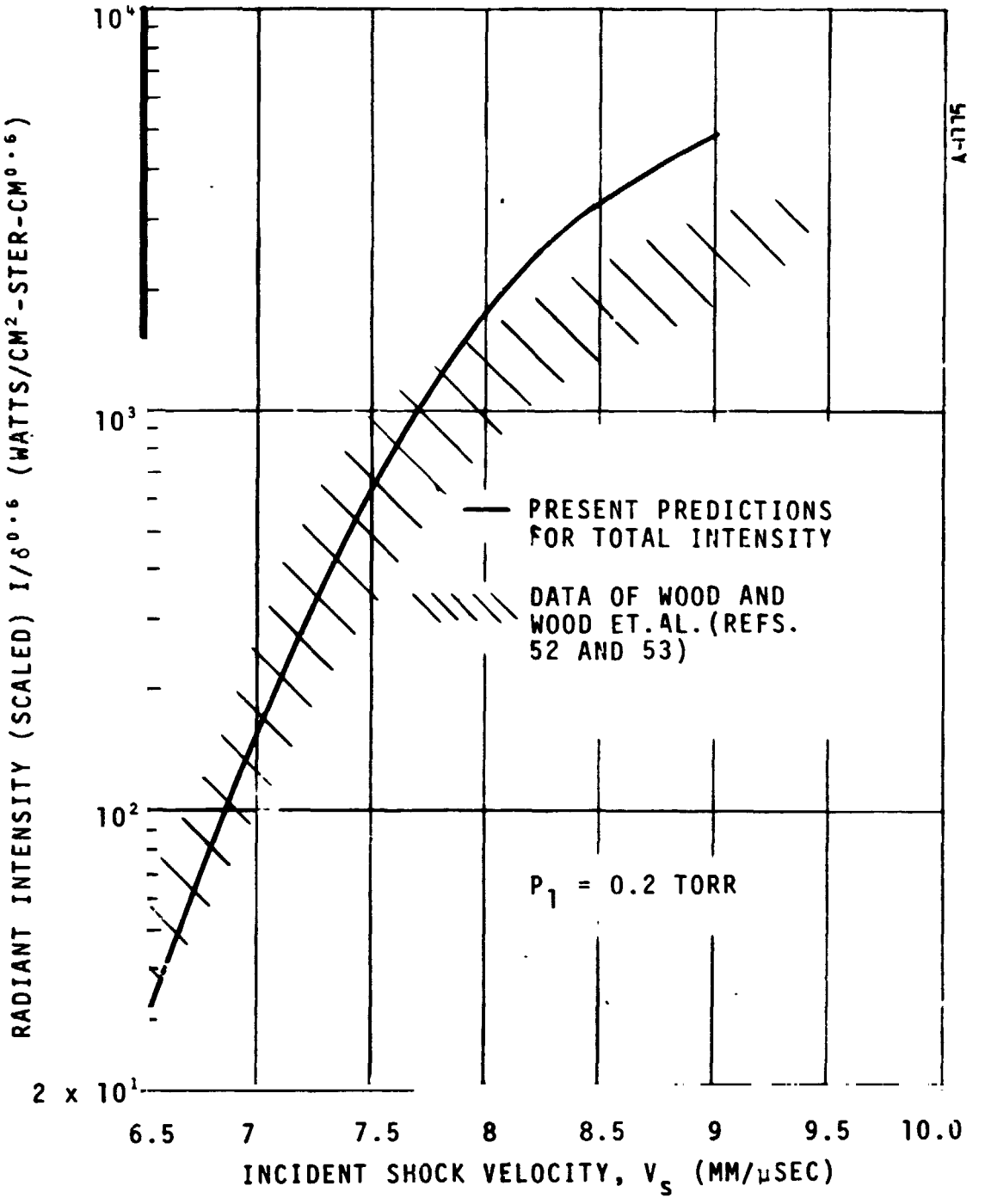

Figure 15. Comparison with Total Intensity Measurements of Wood (Ref. 53) and Wood et.al. (Ref. 52)

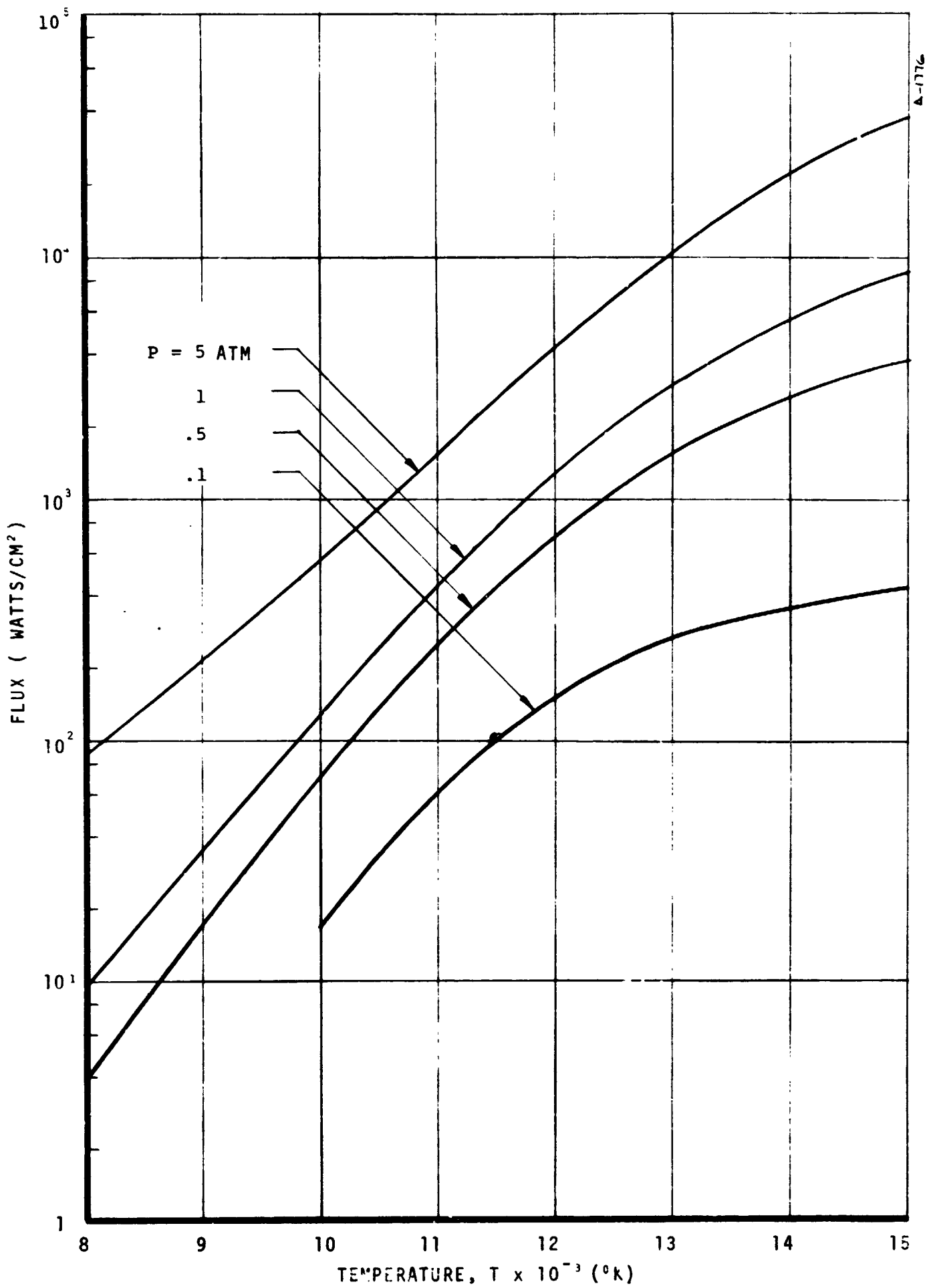

Figure 16. Variation of Flux from a Uniform Air Slab, δ = 1 cm

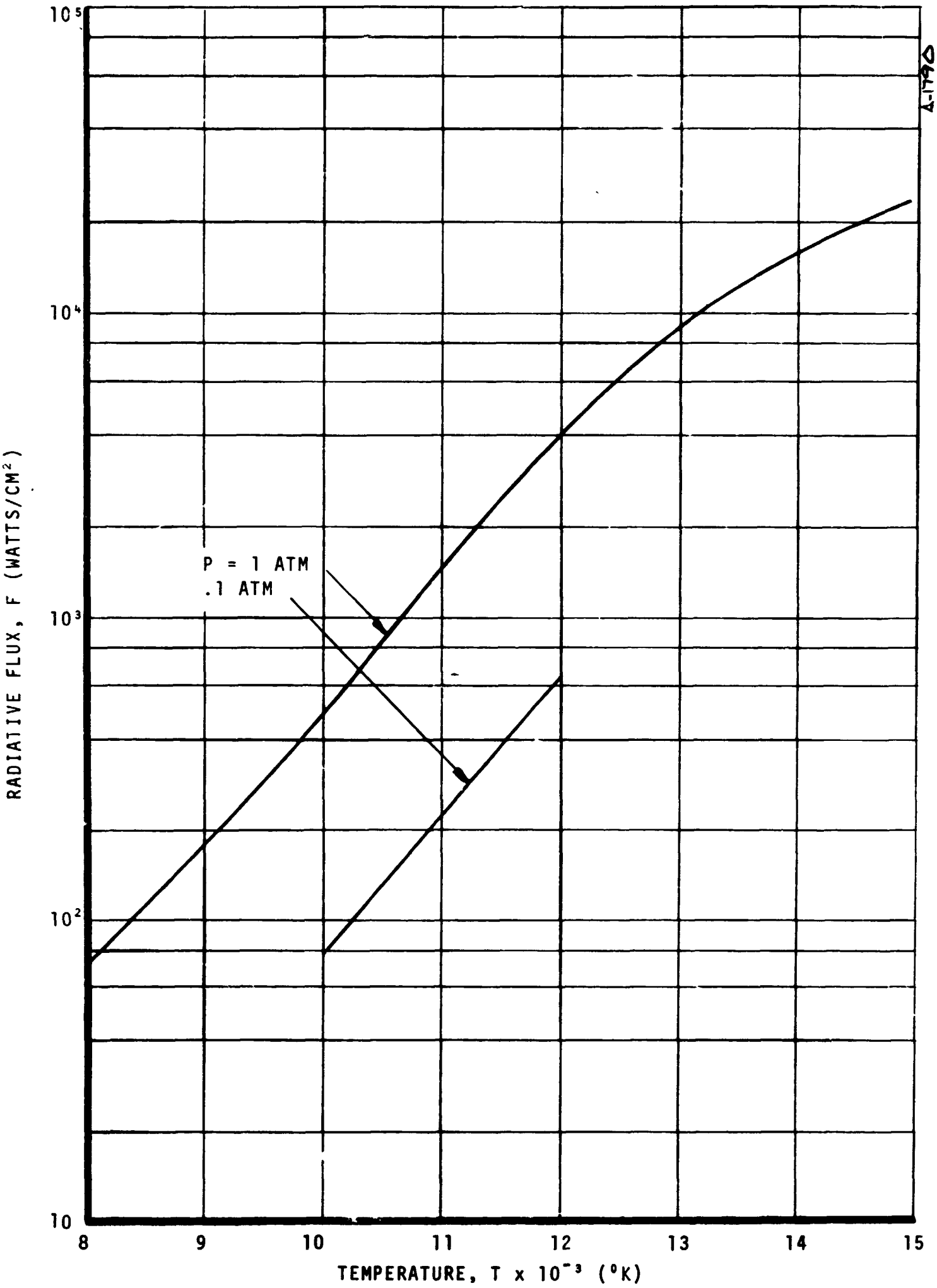

Figure 17. Variation of Flux from a Uniform Air Slab, δ = 10 CM

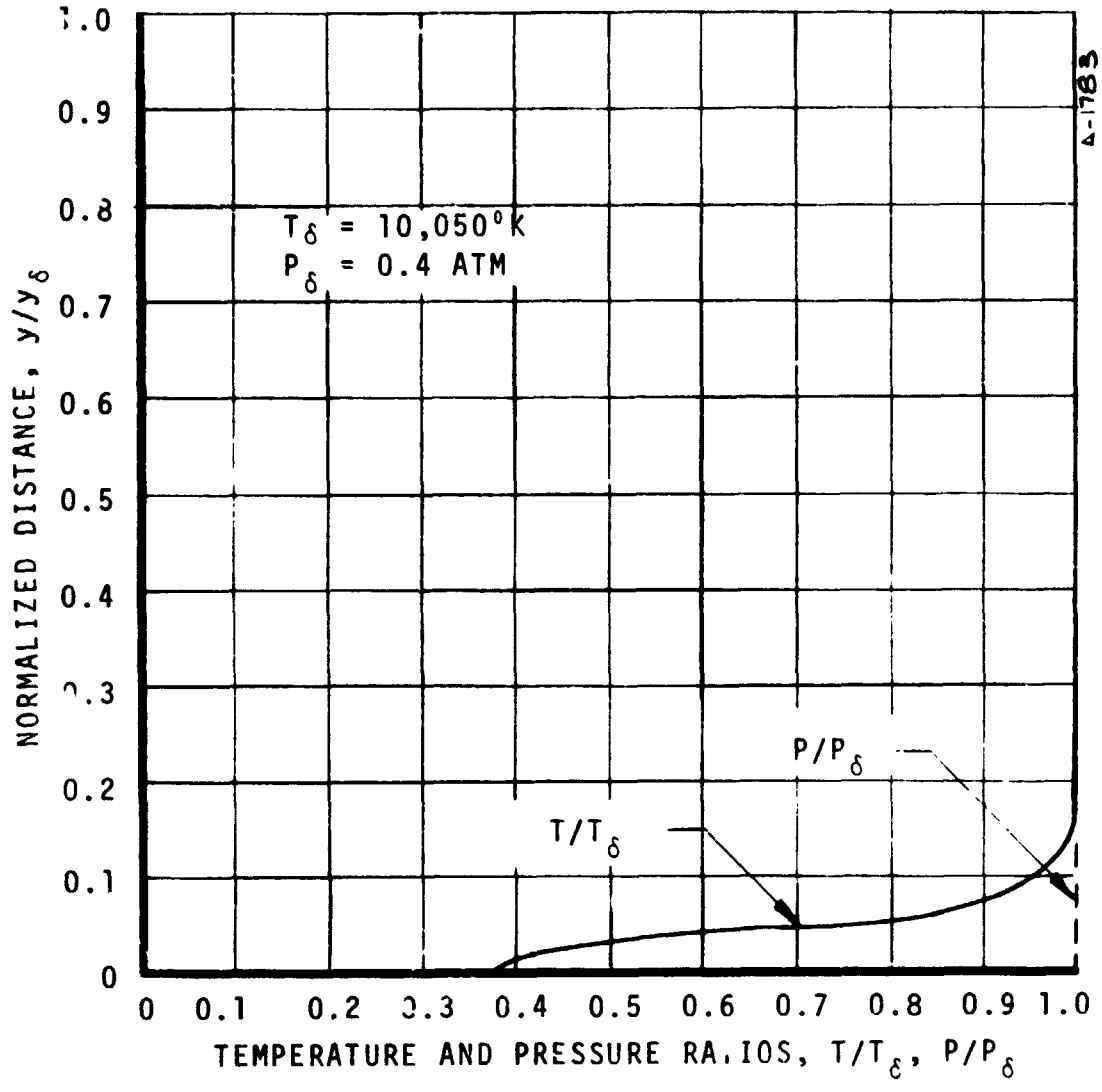

Figure 18. Thermodynamic State Variation

of a vehicle reentering from a lunar mission. Carbon and hydrogen gases were included as they are usually present due to mass injection from the surface of the vehicle.

The spatial distribution of the radiation species is given in Figure 19. The molecules reside in a narrow region immediately adjacent to the wall ($y/y_\delta < 0.01$). In this case the region was so narrow that it had essentially no interaction with the radiation field. A mixing region exists further out where transition from mainly atomic to mainly molecular species occurs ($0.01 < y/y_\delta < 0.1$). The species in this region tend to emit in the visible and absorb in the ultraviolet. Note that atomic carbon and hydrogen are present in significant quantities. The exterior field ($y/y_\delta > 0.1$) consists of pure air species. In this case, the atomic species dominate with the N contributions being of particular importance.

The spectral distribution of the positive continuum fluxes (directed toward the wall) are shown in Figure 20, both at the wall and at the edge of the boundary layer (which is set arbitrarily at $y/y_\delta = 0.211$). The peaks in the wall flux at $h\nu = 1$ ev and 3.3 ev are primarily due to emission from the red and violet CN bands in the boundary layer. There is also a peak in the boundary flux at $h\nu = 3.3$ ev, but this must be attributed to $N_2^+(1-)$ emission from the exterior flow region. The ultraviolet contributions to the boundary flux above 10.8 ev are due to N emission from its photoionization edges with the flux levels beyond 12 ev being nearly black body. Note that the wall flux has undergone severe attenuation in the region $h\nu > 11.5$ ev. This is due to absorption by the photoionization edges of the carbon atoms in the mixing region. Typically, large fractions of the incident ultraviolet continuum will be absorbed in the boundary layer.

The spectral distribution of the wall flux is presented again in Figure 21, but here the line contributions are also included (and presented in terms of averages over arbitrarily specified frequency increments). The line contribution is extremely important (probably dominant) in the visible region. In the ultraviolet region the lines contribute a modest addition to the flux in the 9-10.8 ev range. However, the line contribution in the 10.8-11.5 ev range is negative (dark lines) and the total flux to the wall is significantly less than it would have been if line contributions had not been included. This is also typical as the ultraviolet lines can be strongly absorbed in noniso-thermal regions.

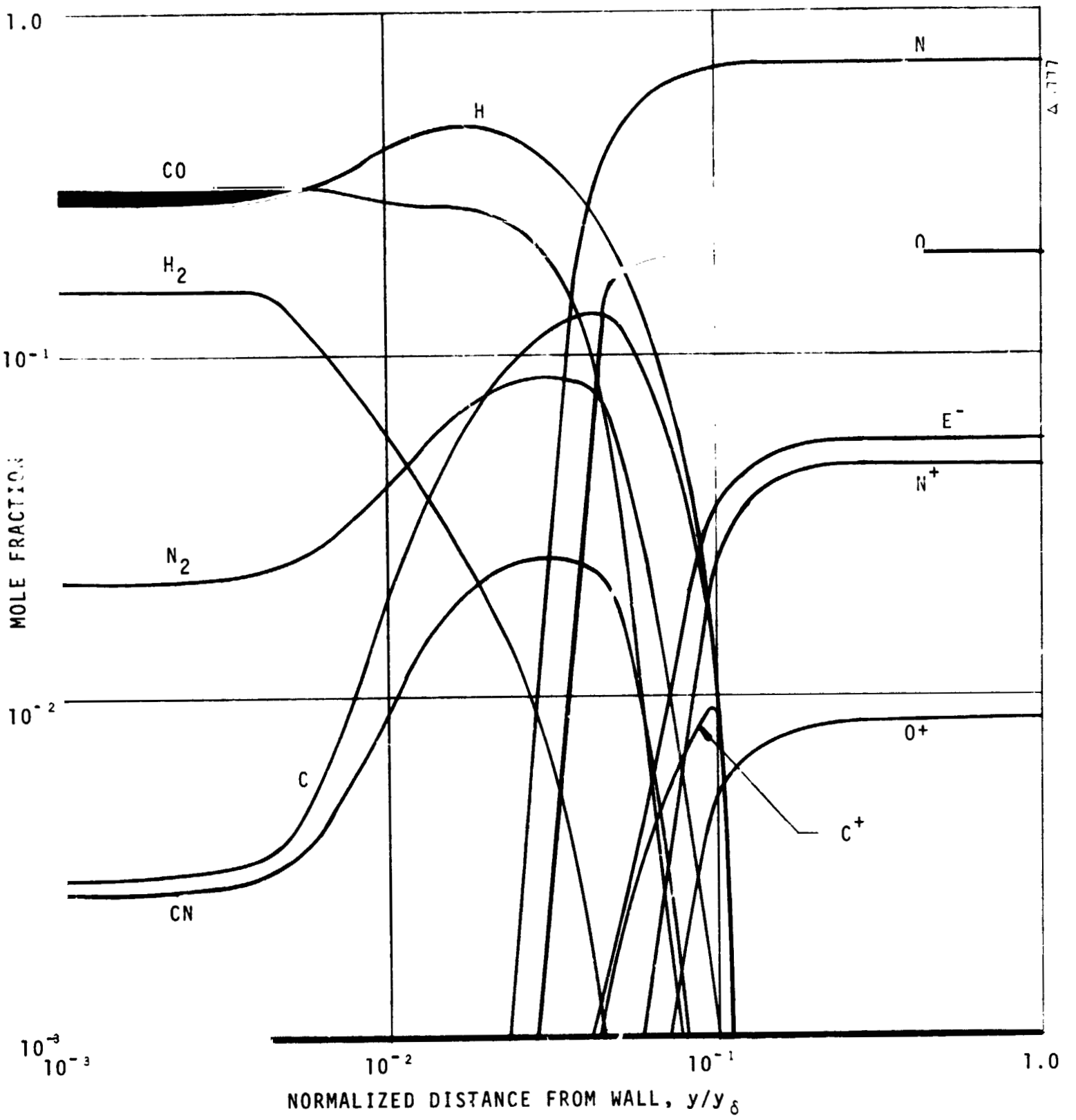

Figure 19. Spatial Distribution of Radiating Species

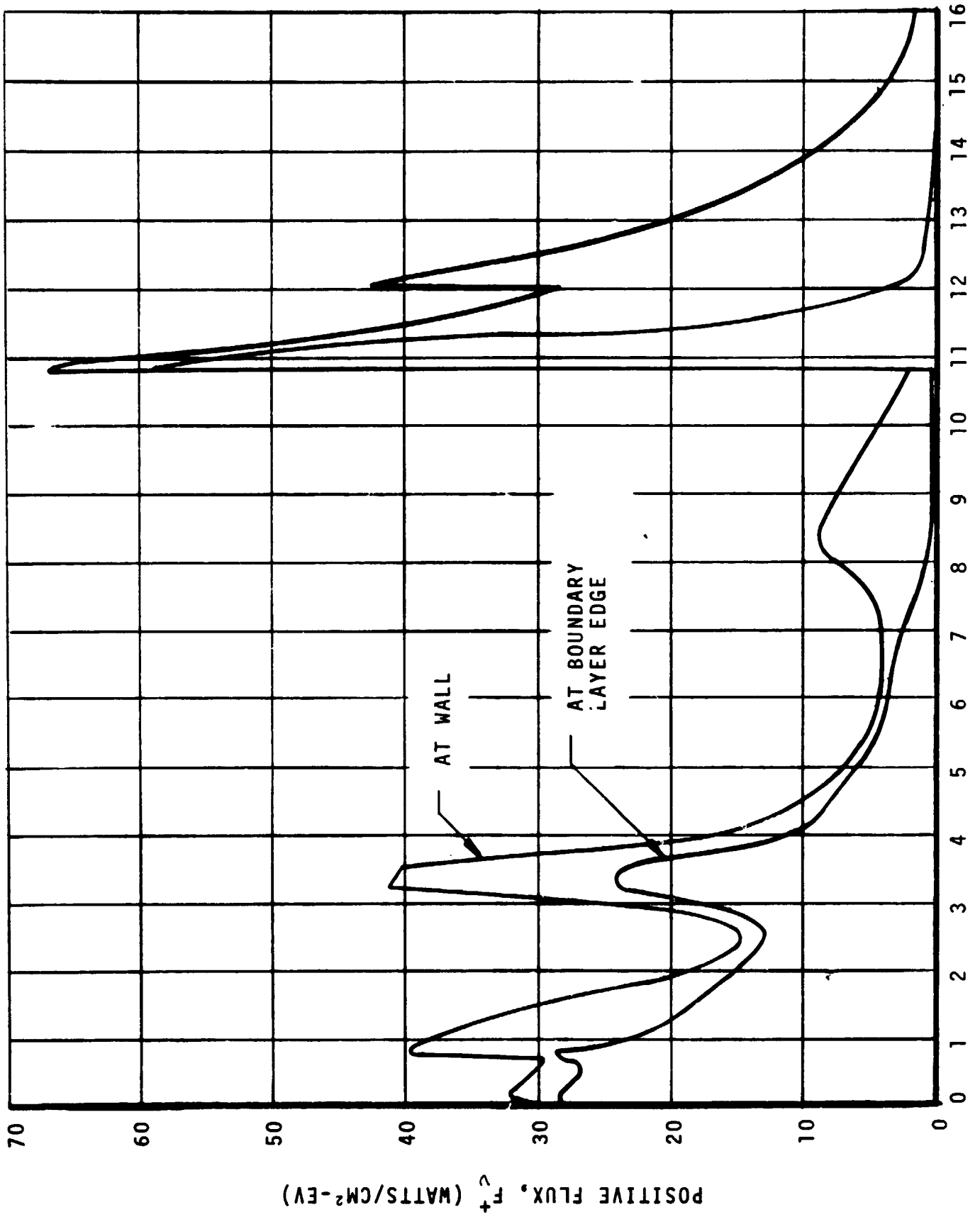

Figure 20. Spectral Distribution of Continuum Fluxes

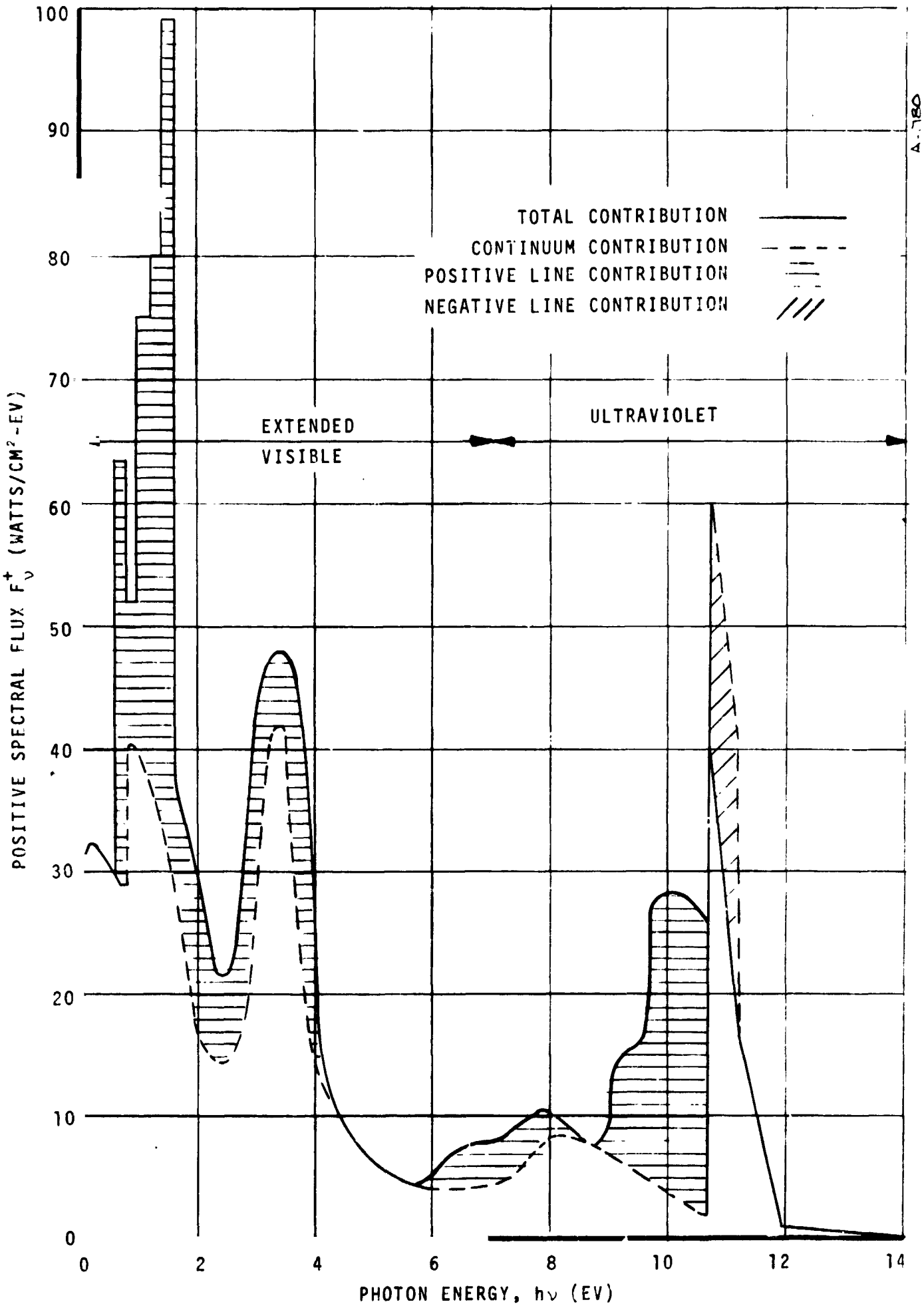

Figure 21. Spectral Variation of Positive Flux at Wall

The energy exchange mechanism between the boundary layer and the exterior flow is illustrated further in Figures 22 and 23. The spatial variation of the transmitted fraction of the positively directed total flux and the relative fractions of its constituents are shown in Figure 22. Thus, the positive flux undergoes a steady attenuation from $\eta \approx 6$ to $\eta \approx 0.75$ with the ultraviolet continuum accounting for the bulk of the loss. For $\eta < 0.75$ the loss rate increases noticeably due to line attenuation. The effect is further illustrated in Figure 23 where the spatial variation of the net flux is shown. The region $6 < \eta < 0.7$ shows that the entering flux is always less than the departing flux causing radiative cooling. Nearer the wall ($\eta < 0.7$) the effect reverses causing radiative heating. Thus, the following qualitative effects are present: (a) the gases near the wall are heated, (b) the gases in the outer regions of the boundary layer are cooled, (c) the emission from the ablated species in the boundary layer is not sufficient to offset the losses from the boundary flux by absorption and (d) the boundary flux is attenuated significantly (in this case by 25 percent) before it reaches the wall.

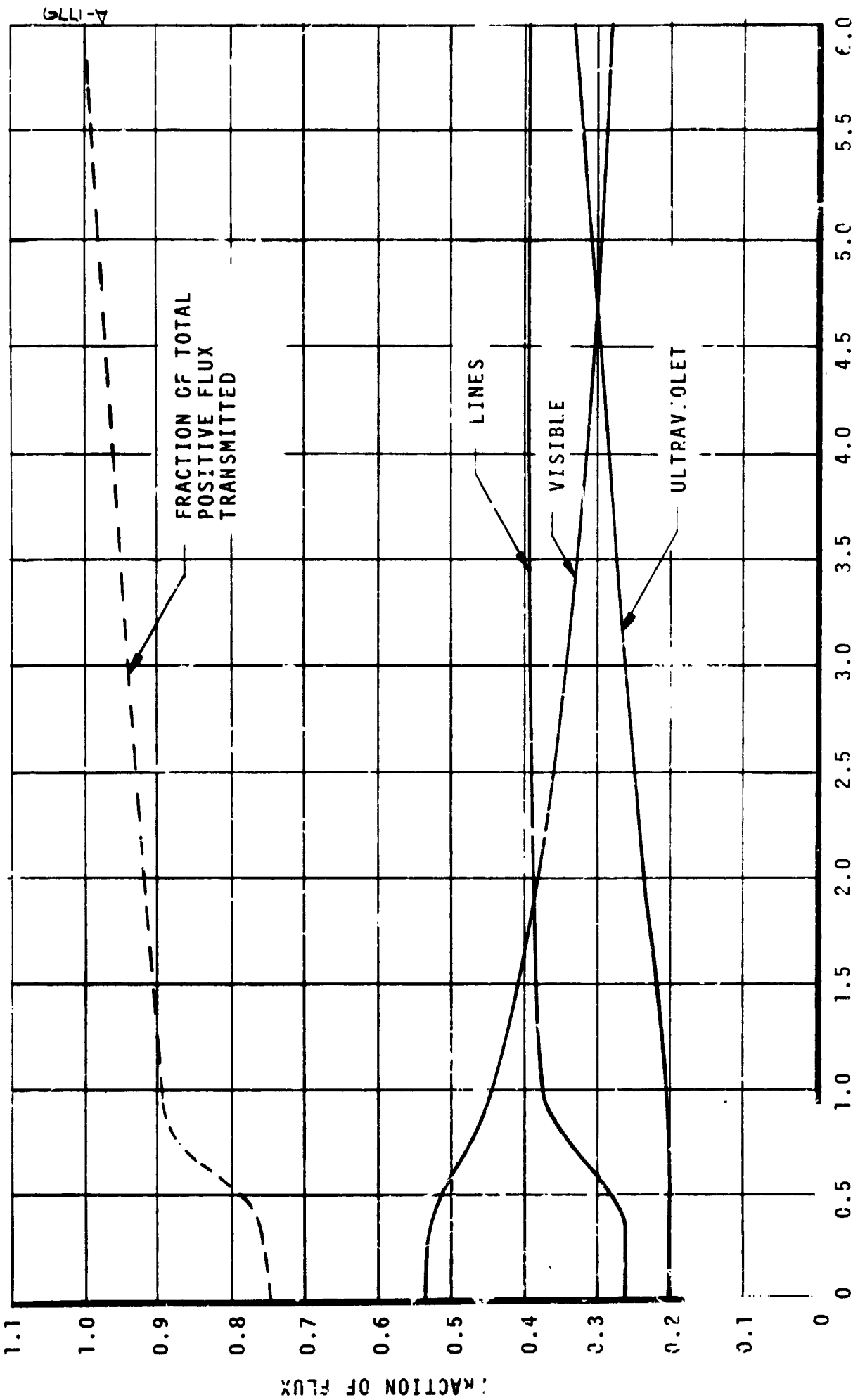

Figure 22. Positive Flux Variation

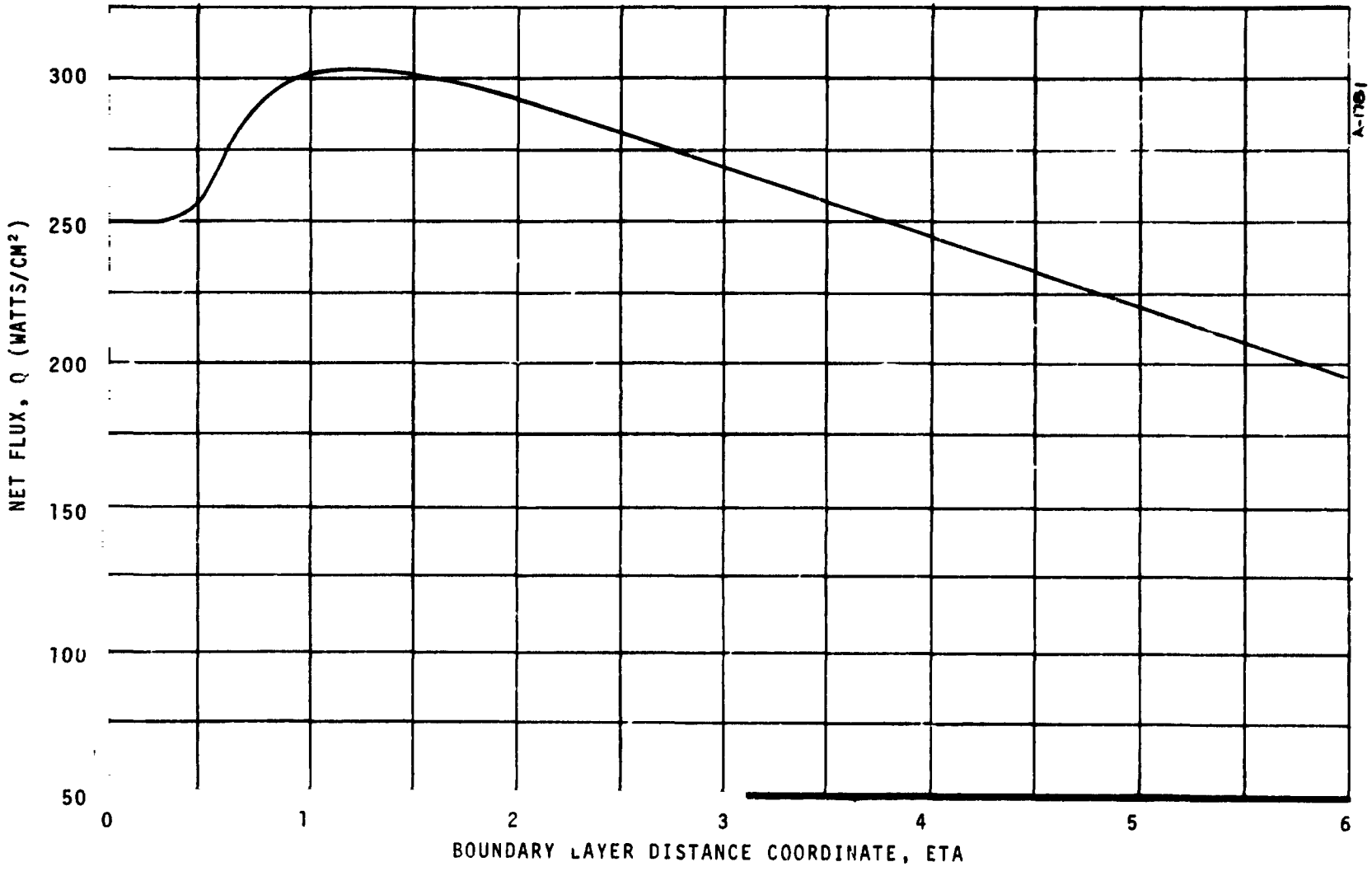

Figure 23. Net Flux (Positive When Directed Toward the Wall)

SECTION 5

CONCLUDING REMARKS

A prediction method has been described which can be used to obtain fluxes or intensities at any specified point within a plane-parallel slab (for the flux calculation) or at any point on a ray (for the intensity calculation). While the method was developed for the study of radiation heating phenomena within the mass injected boundary layer environment, it is not limited to such studies. Indeed, its primary virtue is its versatility. The only approximation which is an integral part the method is the smeared line model for the molecular bands. Any of the other aspects of the properties model can easily be made to include more (or less) detail, allowing important trade-offs to be made between accuracy and computational effort.

The comparisons presented in Sections 4.1 and 4.2 showed that the present predictions are in generally good agreement with predictions from other studies. Comparison with available experiments yielded no additional information as the inconsistencies between the different sets of experimental data are greater than are those between the sets of predictions. However, it was possible to conclude that N^- transition does not necessarily improve the properties model.

Several examples were given in Sections 4.3 and 4.4 which serve to further illustrate the versatility of the method. Additional predictions were presented in Part I of this series of reports and include a prediction of a radiation coupled, mass-injected boundary layer flow.

SECTION 6

REFERENCES

1. Karzas, W.J. and Latter, R.: Electron Radiative Transitions in a Coulomb Field. Astrophys. J.Supplement, 6, 167, 1961.

2. Wilson, K.H. and Nicolet, W.E.: Spectral Absorption Coefficients of Carbon, Nitrogen and Oxygen Atoms. JQSRT, 7, 891, 1967.

3. Lasher, L.E., Wilson, K.H. and Greif, R.: Radiation from an Isothermal Hydrogen Plasma at Temperatures Up to 40,000°K. Lockheed MSC Report No. 6-76-66-17, Revised, July 1967.

4. Burgess, A. and Seaton, M.J.: A General Formula for the Calculation of Atomic Photo-Ionization Cross Sections. Mon. Not. R. Astr. Soc., 120, 121, 1961.

5. Armstrong, B.H., Johnston, R.R., and Kelly, P.S.: Opacity of High Temperature Air. Lockheed Missiles & Space Co., Report No. 8-94-64-2 (also Air Force Weapons Lab. Report AFWL-tr 65-17), 1964.

6. Biberman, L.M. and Norman, G.E.: Recombination Radiation and Bremsstrahlung of a Plasma. JQSRT, 3, 221, 1963.

7. Hahne, G.E.: The Vacuum Ultraviolet Radiation from N^+ and O^+ Electron Recombination in High Temperature Air. NASA TND-2794, June 1965.

8. Biberman, L.M., Vorob'ev, V.S., Norman, G.E., and Iakubov, I.T.: Radiation Heating in Hypersonic Flow. Kosmich, Issled., Vol. 2, No. 3, 1964, pp. 441-454.

9. Griem, H.R.: Plama Spectroscopy. McGraw-Hill Book Co., New York, 1964.

10. Wilson, K.H. and Greif, R.: Radiation Transport in Atomic Plasmas. Lockheed MSC Report No. 6-77-67-31, November 1967.

11. Page, W.A., Compton, D.L., Borucki, W.J., Ciffone, D.L., and Cooper, D.M.: Radiative Transport in Inviscid Nonadiabatic Stagnation-Region Shock Layers. AIAA Paper No. 68-784, June 1968.

12. Condon, E.U. and Shortley, G.H.: The Theory of Atomic Spectra. Cambridge University Press, London, 1935.

13. Griem, H.R., Kolb, A.C., and Shen, R.V.: Start Broadening of Hydrogen Lines in Plasma. NRL Report 5455, 1960.

14. Griem, H.R.: Stark Broadening of Higher Hydrogen and Hydrogenlike Lines by Electrons and Ions.: Astrophys. J., 132, 883, 1960.

15. Hunt, B.L. and Sibulkin, M.: Radiation Transfer in a Gas of Uniform Properties in Local Thermodynamic Equilibrium, Part I, Part II, Part III. Brown Univ. Report No. NONR-562(35)/18, December 1966.

16. Armstrong, B.H.: Apparent Positions of Photoelectric Edges and the Merging of Spectrum Lines. JQSRT, 4, 207, 1964.

17. Vorobyov, V.S. and Norman, G.E.: Energy Radiated in Spectral Lines by an Equilibrium Plama, II. Optics & Spec., 14, 96, 1963.

18. Aroeste, H., and Magee, J.L.: Thermal Radiation Phenomena, Volume 3, Tables of Radiative Properties of Air. Lockheed Report LMSC 3-27-67-1, Vol. 3, May 1967.

19. Biberman, L.M., Mnatsakanyan, A.Kh.: Optical Properties of Air in the Temperature Range from 4,000 to 10,000°K. Teplotizika Vysokikh Temperatur, 4, 148, 1966.

20. Churchill, D.R., Hagstrom, S.A. and Landshoff, R.K.M.: The Spectral Absorption Coefficient of Heated Air. JQSRT, 4, 291, 1964.

21. Lofthus, A.: The Molecular Spectrum of Nitrogen, Spectroscopic Report No. 2, Dept. of Physics, University of Oslo, Blindern, Norway, 1960.

22. Gilmore, F.S.: The Contribution of Generally-Neglected Band Systems and Continua to the Absorption Coefficient of High-Temperature Air. JQSRT, 5, 125, 1965.

23. Watanabe, K., J. Chem. Phys., 22, 1954.

24. Appleton, J.P. and Steinberg, M.: Vacuum-Ultraviolet Absorption of Shock-Heated Vibrationally Excited Nitrogen. J.Chem, Phys., 46, 1521, 1967.

25. Allen, R.A.: Radiation Graphs, Spectrally Integrated Fluxes Including Line Contributions and Self-Absorption. AVCO Research Report 230, September 1965.

26. Churchill, D.R., Armstrong, B.H. and Mueller, K.G.: Absorption Coefficients of Heated Air: A Compilation to 24,000°. Lockheed Report 4-77-65-1, 1965.

27. Arnold, J.O., Reis, V.H., and Woodward, H.T.: Studies of Shock-Layer Radiation of Bodies Entering Planetary Atmospheres. AIAA 2, 2019, 1965.

28. Woodward, H.T.: Predictions of Shock-Layer Radiation from Molecular Band Systems in Proposed Planetary Atmospheres. NASA Technical Note, NASA TN D-3850, Ames Research Center, Moffett Field, California, February 1967.

29. Main, R.P., and Bauer, E.: Opacities of Carbon-Air Mixtures at Temperatures from 3000-10,000°K. JQSRT, 6, 1, 1966.

30. Weisner, J.D.: Hardening Technology Studies-II, Volume III, Aerothermodynamics; Part III, Radiative Properties. Report LMSC-B130391, Vol. III, Part III, Lockheed Missiles & Space Co., Sunnyvale, California, September 1966.

31. Evans, J.S. and Schexnayder, C.J., Jr.: An Investigation of the Effect of High Temperature on the Schumann-Runge Ultraviolet Absorption Continuum of Oxygen. NASA Tech. Report R-92, 1961.

32. Chandrasekhar, S. and Elbert, D.D.: On the Continuous Absorption Coefficient of the Negative Hydrogen Ion. V. Astrophys. J., 128, 114, 1958.

33. John,T.L.: Monthly Notice Ray Astron. Soc., 128, 93, 1964; also 131, 315, 1966.

34. Ohmura, H. and Ohmura, T.: Astrophys. J., 131, 8, 1960; Phys. Rev. 121, 513, 1961.

35. Cooper, J.W. and Martin, J.B.: Phys. Rev., 126, 1482, 1962.

36. Seman, M. and Branscomb, L.M.: Phys. Rev., 125, 1602, 1962.

37. Norman. G.E.: The Role of the Negative Nitrogen Ion N^- in the Production of the Continuous Spectrum of Nitrogen and Air Plasmas. Opt. Spectry., 17, 94, 1964.

38. Boldt, G.: The Recombination of "Minus" Continua of Nitrogen Atoms. Z. Physik 143, 330, 1959.

39. Morris, J.E., Bach, G.R., Krey, R.U., Liebermann, R.W. and Yos, J.M.: Continuum Radiated Power for High-Temperature Air and Its Components, AIAA J., 4, 1223, 1966.

40. Meyerott, R.E., Sokoloff, J., and Nicholls, R.A.: Absorption Coefficients of Air. Report No. LMSC-288052, Lockheed Missiles & Space Co., Sunnyvale, California, September 1959. Also, Geophysics Res. Dir., GRO TR-60-277.

41. Kendall, R.M.: A General Approach to the Thermochemical Solution of Mixed Equilibrium-Nonequilibrium, Homogeneous or Heterogeneous Systems. Aerotherm Final Report No. 66-7, Part V, March 14, 1967.

42. Hochstim, A.R.: Equilibrium Compositions, Thermodynamic and Normal Shock Properties of Air with Additives. General Dynamics, Convair Report ZPH-122, 1961.

43. Gilmore, F.R.: Thermal Radiative Phenomena, Vol. 1, The Equilibrium Thermodynamic Properties of Air. Lockheed Report 3-27-67-1, Vol. I, May 1967.

44. Gilmore, F.R.: Energy Levels, Partition Functions and Fractional Electronic Populations for Nitrogen and Oxygen Atoms and Ions to 25,000°K, RAND Corp. RM-3748-PR, 1963.

45. Wiese, W.L., Smith, M.W., and Glennon, B.M.: Atomic Transition Probabilities. National Bureau of Standards Report NSRDS-4, 1966.

46. Nicolet, W.E.: User's Manual - Radiation Transfer Code (RAD). Report No. 68-39, Aerotherm Corporation, Mountain View, California, October 15, 1968.

47. Allen, R.A.: Air Radiation Tables: Spectral Distribution Functions for Molecular Band Systems. Research Report 236, AVCO-Everett Research Laboratory, Everett, Massachusetts, April 1966.

48. Sherman, M.P. and Kulander, J.L.: Free-Bound Radiation from Nitrogen, Oxygen and Air. General Electric Co. Report R65SD15, May 1965.

49. Kelly, P.S.: Transition Probabilities in Nitrogen and Oxygen from Hartree-Fork-Slater Wave Functions. JQSRT, 4, 117, 1964.

50. Nerem, R.M.: Stagnation Point Heat Transfer in High Enthalpy Flows. Ohio State Univ. Report FDL-TDR-64-41, Part II, March 1964.

51. Gruszczynski, J.S. and Warren, W.R.: Study of Equilibrium Air Total Radiation. AIAA Paper No. 66-103, January 1966.

52. Wood, A.D., Hoshizaki, H., Andrews, J.C., and Wilson, K.H.: Measurements of the Total Radiant Intensity of Air. AIAA Paper No. 67-311, April 1967.

53. Wood, A.D.: Private communication.

54. Golobic, R.A., and Nerem, R.M.: Shock-Tube Measurements of End-Wall Radiative Heat Transfer in Air. AIAA J., 6, 1741, 1968.